

AD-A170 639

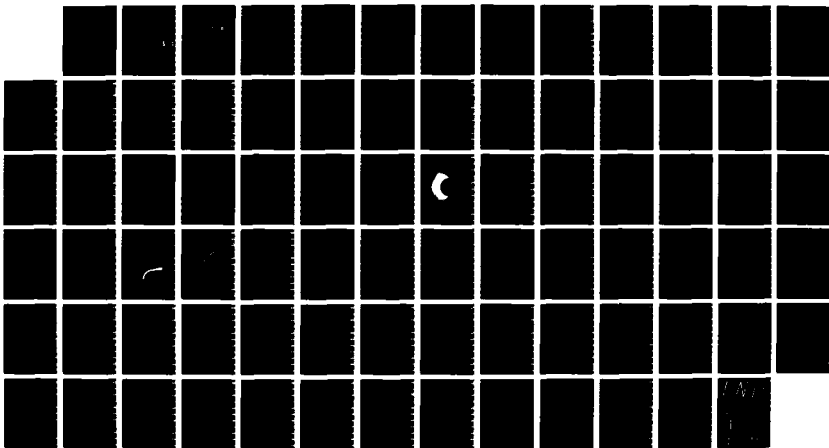
NUMERICAL STUDY OF HIGH SPEED VISCOUS FLOWS(U) AIR
FORCE INST OF TECH WRIGHT-PATTERSON AFB OH SCHOOL OF
ENGINEERING K B JOCHUM DEC 86 AFIT/BAE/AA/86D-4

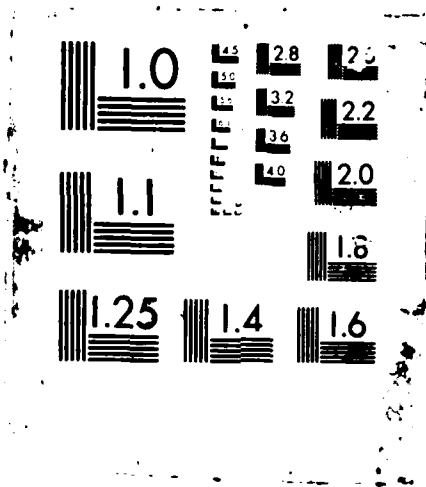
1/1

UNCLASSIFIED

F/G 28/4

ML





①

AD-A178 639

DTIC FILE COPY



NUMERICAL STUDY
 OF
 HIGH SPEED VISCOUS FLOWS

THESIS

Keith B. Jochum
 Captain, USAF

AFIT/GAE/AA/86D-4

DTIC
 ELECTE
 APR 03 1987
 S
 D

DISTRIBUTION STATEMENT A
 Approved for public release;
 Distribution Unlimited

DEPARTMENT OF THE AIR FORCE
 AIR UNIVERSITY
AIR FORCE INSTITUTE OF TECHNOLOGY

Wright-Patterson Air Force Base, Ohio

87 4 2 042

①

DTIC
ELECTE
APR 03 1987
S D D

NUMERICAL STUDY
OF
HIGH SPEED VISCOUS FLOWS

THESIS

Keith B. Jochum
Captain, USAF

AFIT/GAE/AA/86D-4

Approved for public release; distribution unlimited

NUMERICAL STUDY OF HIGH SPEED VISCOUS FLOWS

THESIS

Presented to the Faculty of the School of Engineering
of the Air Force Institute of Technology

Air University

In Partial Fulfillment of the
Requirements for the Degree of
Master of Science in Aeronautical Engineering



Keith B. Jochum, B.S.
Captain, USAF

December 1986

Accession For	
NTIS CRA&I	<input checked="" type="checkbox"/>
DTIC TAB	<input type="checkbox"/>
Unannounced	<input type="checkbox"/>
Justification	
By	
Date	
Availability Codes	
Dist. Statement	
A-1	

Preface

Within the past 5-7 years, the ability to model the supersonic/hypersonic viscous flows using Computational Fluid Dynamics (CFD) techniques has advanced considerably. An algorithm due to Dr. James Thomas of NASA Langley Research Center, Hampton, Virginia, was used in the current study for performing accurate and efficient flow field calculations over blunt bodies. For high speed flow, the physics of the flow can be modeled using the Approximate Navier-Stokes (ANS) equations. A relaxation type algorithm is developed in the present work for solving the ANS equations and solutions are obtained for some model problems.

I would like to thank Dr. A. Halim for supervising this study and for his technical assistance and aid with this research. I wish to thank Mr C. Rumsey of the NASA Langley Research Center for checking the Thomas code on the NASA Ames Cray II. I also wish to thank Capt Carlson, for writing the block tridiagonal matrix solver used in the ANS algorithm.

During this study I used the Cyber and Cray XMP computers at WPAFB, OH for the computational results presented in this thesis. I also used an Amiga personal computer, with Textcraft word processing software to write this thesis. The thesis was printed on a Juki 5510 printer.

Table of Contents

	Page
Preface	ii
List of Figures	v
List of Symbols	vi
Abstract	ix
I. Introduction	1
II. Analysis	6
Governing Equations	6
Coordinate Transformation	9
Approximate Navier-Stokes Equations	11
III. Numerical Solutions of the Equations	14
Fully Implicit Scheme	14
The Upwind Relaxation Scheme	16
Viscous Flux Vector Differencing	19
IV. Results and Discussions	21
The Blunt Body Flow	21
Supersonic Flow Past Circular Wedge	30
One Dimensional Couette Flow	38
Supersonic Flow Over Flat Plate	42
V. Conclusions and Recommendations	46
Appendix A: Coordinate Transformation of Governing Equations	47
Appendix B: Details about the Upwind Relaxation Scheme	51
Linearizations of the ANS Equations	51

Finite Difference Equations	52
Jacobian Matrices	55
Bibliography	64
VITA	67

List of Figures

Figure		Page
1.	Typical grid for the Blunt Body problem . .	23
2.	Comparison of Wall Pressure	24
3.	Comparison of Heat Flux	25
4.	Mach Contours For Blunt Body	26
5.	Velocity Vectors For Blunt Body	27
6.	Density Contours For Blunt Body	28
7.	Pressure Contours For Blunt Body	29
8.	Clustered grid for the Circular Wedge	32
9.	Density Contours For Circular Wedge	33
10.	Mach Contours For Circular Wedge	34
11.	Wall Pressure For Circular Wedge	35
12.	Distribution of the horizontal velocity at the outflow plane	36
13.	Distribution of the vertical velocity at the outflow plane	37
14.	Accuracy study of Couette flow for different pressure gradients (B)	40
15.	Velocity Profiles For Couette Flow	41
16.	Comparison of Velocity Profiles For Flat Plate	44
17.	Comparison of Temperature Profiles For Flat Plate	45

List of Symbols

c	speed of sound
c_p	specific heat at constant pressure
D	diameter
E	vector of inviscid terms that are differentiated with respect to coordinate tangent to the body
E_v	vector of viscous terms that are differentiated with respect to coordinate tangent to the body
e	internal energy
e_t	total energy
η	coordinate in computational space normal to the body
F_n	vector of inviscid terms that are differentiated with respect to vertical coordinate normal to the body
F_v	vector of viscous terms that are differentiated with respect to vertical coordinate normal to the body
γ	ratio of specific heats
J	transformation Jacobian
k	coefficient of conductivity
L	reference length
M	local Mach number
μ	coefficient of viscosity
ω	coefficient used to split the streamwise pressure
F	vector of the split pressure differentiated with respect to streamwise coordinate tangent to the body
p	pressure
Pr	Prandtl number

\mathbf{E}	vector defined in equation (17)
q	heat flux
R	gas constant
Re	freestream Reynolds number
ρ	density
σ	arbitrary safety factor used in equation (48)
T	local temperature
t	time
τ	shear stress
u	velocity component tangent to the body
V	fluid velocity
v	velocity component normal to the body
x	coordinate in physical space tangent to the body
ξ	coordinate in computational space tangent to the body
y	coordinate in physical space normal to the body

Superscript

\cdot	denotes dimensional variables
\cdot	denotes vectors transformed to general coordinates

Subscripts

stag	denotes stagnation point conditions
w	denotes wall conditions
∞	denotes freestream condition
η	partial derivative with respect to η
t	partial derivative with respect to time

x partial derivative with respect to x
 ξ partial derivative with respect to ξ
y partial derivative with respect to y

Abstract

Thermal deformations induced by aerodynamic heating on high speed vehicles are an important concern in design. Aerodynamic heating may have a significant effect on the performance of the vehicle, and effective techniques for predicting the heat transfer and flow properties are required. The accuracy of numerical solutions depend on the grid used. Usually accurate prediction requires clustering of grid points near the surface of the body. Using an explicit algorithm to solve such problems results in the requirement for very small time steps in order to satisfy the stability bounds. Therefore, many iterations and large computer times are required to reach the steady state. To remove the time step restriction, fully implicit methods have been investigated. Results for high speed flow past a circular wedge using an implicit flux splitting scheme are shown. Also viscous blunt body flows are computed, and qualitative comparisons with existing experimental data are given. In an effort to decrease the computational costs associated with the implicit algorithms for the Navier-Stokes equations, a relaxation algorithm is developed for the Approximate Navier-Stokes (ANS) equations. Results for Couette flow and supersonic flow over a flat plate are obtained using this relaxation algorithm and compared to analytical and other numerical solutions.

NUMERICAL STUDY OF HIGH SPEED VISCOUS FLOWS

I Introduction

The accurate prediction of the flow field and heating environment about advanced flight vehicles at high altitude has been the aim of recent research efforts. Previously, the inviscid flow around such vehicles has been computed by solving the Euler equations (1-5). In order to account for viscous effects, the inviscid solutions have been coupled with matching boundary-layer analysis. However for problems with very strong interaction between the viscous and inviscid portions of the flow domain as in the case when the viscous layer and the shock layer are completely merged, the classical ways of using the boundary-layer interaction methodology breaks down. On the otherhand, the full Navier-Stokes (NS) equations or the Approximate Navier-Stokes (ANS) equations have shown great promise in predicting the complete inviscid-viscous flow field around shuttle-like bodies as well as more realistic shuttle body shapes.

Within the last 5-7 years, the ability to model the supersonic/hypersonic flow over complex geometry configurations using Computational Fluid Dynamics (CFD) techniques has advanced considerably. The current work is an initial stage of developing a computational capability of modeling the aerothermodynamic environment about advanced

flight vehicles in high altitude regimes where nonequilibrium chemistry effects are important. The perfect gas assumption has been used for the present investigation. Different approaches are available for solving such problems. The NS formulations lead to a nonlinear system of equations. Using an explicit algorithm to solve such problems results in the requirement of very small time-steps in order to satisfy the stability bounds. Therefore, many iterations and large computer times are required to reach the steady state. To remove the time-step restriction, fully implicit methods have been investigated. The fully implicit code used in this study for solving high speed viscous flows is described in reference (19). The algorithm uses implicit upwind finite volume flux vector splitting on the inviscid terms and second order central differencing on the viscous terms. An attractive feature of upwind flux vector splitting schemes is that they are naturally dissipative, and artificial viscosity terms are no longer required to overcome instabilities in regions of strong gradients. Use of the conservation law form of the governing equations in this algorithm also allows shocks to be captured, and eliminates the need to use shock-fitting techniques to obtain the location and strength of the shocks in the flow (7:1).

The inviscid flux vectors are split into forward and backward flux vectors by splitting the eigenvalues of the Jacobian matrix into positive and negative diagonal

eigenvalue matrices. These flux vectors are then differenced using the appropriate upwind or downwind scheme (7:1-2).

The algorithm will be used to compute two hypersonic viscous flows over blunt bodies using the full NS equations. Results are obtained first for the blunt body flow surrounding a circular cylinder which was studied by Tannehill et. al. (22). The freestream conditions chosen for these computations are $M_\infty=4.6$, $Re_\infty=10000$, $Pr=0.72$, $P_\infty=14.93\text{N/m}^2$, $T=167\text{K}$ and $\gamma=1.4$, with a cylinder diameter (D) of 0.3048 m and a wall temperature of 556K. Comparison with available experimental and numerical data will be given. Solutions also are obtained for supersonic viscous flows past a circular wedge geometry. Qualitative comparisons with solutions of Bey et. al. (10) using other algorithms will be given. Bey et. al. used a finite element algorithm to predict the inviscid flow field around the same geometry.

For high speed flows, the Reynolds number is usually very large and consequently the thickness of the viscous layer is very small. For problems of this class, the solution of the full NS equations is unnecessary and time consuming. Different levels of approximations for the NS equations became the debate within the CFD community.

Boundary-Layer equations, are a simplified form of the NS equations where the pressure gradient normal to the body surface is neglected. Viscous terms with derivatives in the direction tangent to the body are also neglected after an order of magnitude analysis is performed on the NS equations.

The order of magnitude analysis is accomplished by assuming the velocity component normal to the body is small compared to the velocity component tangent to the body. Although the BL equations require much less computational effort than the NS equations, the BL equations are limited to the type of flows they can physically model accurately. Thus an intermediate set of governing equations were developed.

Approximate Navier-Stokes equations(ANS), are also simplified NS equations and like the BL equations neglect viscous terms with derivatives tangent to the body but retain all other terms. An advantage of retaining terms which were neglected in the BL equations, is that separated and reverse flow regions can now be computed (8:421). The ANS equations contain all the Euler equation terms, so that the interaction between the viscous and inviscid regions of the flow are automatically taken into account (16:1). The ANS equations like the BL equations require less computational effort than the NS equations, and derivatives in the direction tangent to the body can be approximated using a technique that marches the solution in the direction tangent to the body.

Upwind relaxation algorithms became an attractive tool to solve the ANS equations and are used by many researchers (25). In the present effort, an upwind pseudo-time relaxation algorithm that globally sweeps over the flow field in the direction tangent to the body, is used to calculate steady state viscous flow solutions. This algorithm is

similar to the work of Thomas and Walter (25), using a first order upwind scheme in the direction tangent to the body and a second order central scheme on all terms in the direction normal to the body.

The first model problem solved using the developed algorithm is the Couette flow problem. This problem was chosen since it has an exact solution. Comparison of the present results with the exact solution provides a test of the validity and correctness of the present analysis and solution procedure. Solutions are then obtained for supersonic flow over a flat plate and comparison with other solutions will be given.

II Analysis

Governing Equations

The time-dependent compressible Navier-Stokes (NS) equations express the conservation of mass, momentum, and energy for an ideal gas in the absence of external forces (25:1). The momentum equations use Newton's viscosity law, and the energy equation uses Fourier's conduction law so that the NS equations can be written in the non-dimensional form in conservation law form and Cartesian coordinates as follows

continuity:

$$\rho_e + (\rho u)_x + (\rho v)_y = 0 \quad (1)$$

x momentum:

$$(\rho u)_e + (\rho u^2 + p - \tau_{xx})_x + (\rho uv - \tau_{xy})_y = 0 \quad (2)$$

y momentum:

$$(\rho v)_e + (\rho uv - \tau_{xy})_x + (\rho v^2 + p - \tau_{yy})_y = 0 \quad (3)$$

energy:

$$\begin{aligned} (\rho e)_e + [(\rho e + p)u - u\tau_{xx} - v\tau_{xy} + q_x]_x + \\ [(\rho e + p)v - u\tau_{xy} - v\tau_{yy} + q_y]_y = 0 \end{aligned} \quad (4)$$

where

$$q_x = -\mu c_x / [\text{RePr}(\gamma - 1)] \quad (5)$$

$$q_y = -\mu c_y / [\text{RePr}(\gamma - 1)] \quad (6)$$

$$\tau_{xx} = (2u_x - v_y)2\mu / 3\text{Re} \quad (7)$$

$$\tau_{xy} = (u_y + v_x)\mu / \text{Re} \quad (8)$$

$$\tau_{yy} = (2v_y - u_x)2\mu / 3\text{Re} \quad (9)$$

$$\text{Re} = \rho^* c^* L^* / \mu^* \quad (10)$$

$$\text{Pr} = c_p^* \mu^* / \kappa^* \quad (11)$$

$$c_p = \gamma R / (\gamma - 1) \quad (12)$$

$$\mu = 1.458 \times 10^{-6} \text{kg} / (\text{ms}(\text{K})^{1/2}) T^{*3/2} / (T^* + 110.4\text{K}) \quad (13)$$

the definitions of variables are given in the List of Symbols and references (8:189) and (8:480-482). The perfect gas equation is used for closure

$$p = (\gamma - 1) \rho e \quad (14)$$

$$T = \gamma p / \rho \quad (15)$$

Equations (1,2,3 and 4) can be combined in vector form and written in the strong conservative form as follows

$$Q_x + (E-E_v)_x + (F_1-F_v)_y = 0 \quad (16)$$

where

$$Q = [\rho, \rho u, \rho v, e_x]^T \quad (17)$$

$$E = [\rho u, \rho u^2+p, \rho uv, (e_x+p)u]^T \quad (18)$$

$$E_v = [0, \tau_{xx}, \tau_{xy}, u\tau_{xx}+v\tau_{xy}-q_x]^T \quad (19)$$

$$F_1 = [\rho v, \rho uv, \rho v^2+p, (e_x+p)v]^T \quad (20)$$

$$F_v = [0, \tau_{xy}, \tau_{yy}, u\tau_{xy}+v\tau_{yy}-q_y]^T \quad (21)$$

. Equations (1-21) have been nondimensionalized using the following identities

$$\begin{array}{lll} t = t^*/L^*/c_{\infty}^* & x = x^*/L^* & y = y^*/L^* \\ u = u^*/c_{\infty}^* & v = v^*/c_{\infty}^* & e = e^*/c_{\infty}^{*2} \\ \rho = \rho^*/\rho_{\infty}^* & T = T^*/T_{\infty}^* & \mu = \mu^*/\mu_{\infty}^* \\ p = p^*/\rho_{\infty}^* c_{\infty}^{*2} & L^* = 1 & c_{\infty}^{*2} = \gamma R T_{\infty}^* \end{array} \quad (22)$$

. The highest order terms come from the viscous forces which are second order, but there are first order convective terms

that are nonlinear. Thus the NS equations are mathematically classified as elliptic partial differential equations (18:139-155). Elliptic means the state of every point in the flow is dependent on the state of every other point in the flow, which requires solving the whole flow field at the same time. That means boundary conditions must be described at every point surrounding the flow domain. Typically for a flow around an aerodynamic body, zero slip conditions are specified on the surface of the body and either the heat flux is specified or the temperature is described along the surface. The second boundary condition is usually taken at the far field, where the undisturbed flow conditions are used. The third boundary condition is applied far downstream of the body where the flow is weakly elliptic so parabolic approximations can be used. The last boundary condition is always described at the inlet of the flow domain which will be the line of symmetry for axisymmetric configurations.

Coordinate Transformation

To make the governing equations usable for a variety of geometries, they can be transformed to general coordinates. The coordinate transformations used on the governing equations are of the following form

$$\xi = \xi(x, y) \quad (23)$$

$$\eta = \eta(x, y) \quad (24)$$

where ξ and η are defined in the List of Symbols. When the above transformation is applied to equation (16) the following equation results

$$Q'_x + E'_\xi + F'_\eta = 0 \quad (25)$$

where

$$J = [\xi_x \eta_y - \xi_y \eta_x] \quad (26)$$

$$Q' = Q/J \quad (27)$$

$$E' = [\xi_x (E - E_\eta) + \xi_y (F_x - F_\eta)] / J \quad (28)$$

$$F' = [\eta_x (E - E_\eta) + \eta_y (F_x - F_\eta)] / J \quad (29)$$

J is the transformation Jacobian. See Appendix A, for details on the transformation of the governing equations into generalized coordinates.

With the NS equations written in generalized coordinates, it is easy to write an algorithm that can compute solutions for a variety of geometries. The method described in reference (19) uses a finite-volume method describing the balance of mass, momentum, and energy over an arbitrary control volume. The vectors ξ_x/J , ξ_y/J , η_x/J and

η_y/J represent directed areas of cell interfaces in the ξ and η directions in computational space. The Jacobian represents the inverse of the cell volume, and the elements $\rho u/J$ and $\rho v/J$ are the mass fluxes crossing the cell interfaces in the ξ and η directions. These fluxes are then split into forward and backward contributions to the flow crossing the cell interfaces, which allows the algorithm to accurately resolve separated and subsonic flow regions (6:2).

Approximate Navier-Stokes Equations

The Approximate Navier-Stokes (ANS) equations are formed from the NS equations, by doing an order of magnitude analysis on the equations after assuming the velocity component normal to the body is much less than the velocity component tangent to the body. After doing this order of magnitude analysis, viscous terms with derivatives in the direction tangent to the body are considered small compared to the viscous terms with derivatives normal to the body. Once this is done equation (25) can be written as

$$Q'_\epsilon + E''_\xi + F''_\eta = 0 \quad (30)$$

where

$$E'' = (\xi_x E + \xi_y F_\Delta) / J \quad (31)$$

$$F'' = [\eta_x (E - E''_{xx}) + \eta_y (F_x - F''_{xy})] / J \quad (32)$$

$$E''_{xx} = [0, \tau''_{xx}, \tau''_{xy}, u \tau''_{xx} + v \tau''_{xy} - q'_{xx}]^T \quad (33)$$

$$F''_{xy} = [0, \tau''_{xy}, \tau''_{yy}, u \tau''_{xy} + v \tau''_{yy} - q'_{xy}]^T \quad (34)$$

$$\tau''_{xx} = (2\eta_x u_\eta - \eta_y v_\eta) 2\mu / 3Re \quad (35)$$

$$\tau''_{xy} = (\eta_y u_\eta + \eta_x v_\eta) \mu / Re \quad (36)$$

$$\tau''_{yy} = (2\eta_y v_\eta - \eta_x u_\eta) 2\mu / 3Re \quad (37)$$

$$q'_{xx} = -\mu \eta_x c_\eta / [RePr(\gamma - 1)] \quad (38)$$

$$q'_{xy} = -\mu \eta_y c_\eta / [RePr(\gamma - 1)] \quad (39)$$

. It has been demonstrated that these ANS equations are applicable to a wide class of problems (25:2).

The main feature of the ANS equations is the fact that the highest derivative in the streamwise direction is less by one than those for NS equations. That means the ANS equations are parabolic for the viscous flow region but they are also hyperbolic for the inviscid flow if it is supersonic. So the equations are actually a mixed set of hyperbolic- parabolic equations. That is the reason the abbreviation ANS was preferred over Parabolized Navier-Stokes

(PNS) or Partially Parabolized Navier-Stokes (PPNS) abbreviations. The ANS equations have recently become famous, because they can predict complex three dimensional, steady, supersonic viscous flow fields in an efficient method. The efficiency for three dimensional solutions came from the fact that the equations can be solved using a space-marching finite difference technique as opposed to the time marching technique normally employed for NS equations. To be able to use the ANS equations, the solution at a certain plane or location in the streamwise direction has to be known as opposed to the NS equations. The details of the numerics are shown in Chapter III.

III Numerical Solution of the Equations

The important aspects concerning the numerical solution of the governing equations are discussed in this chapter. The finite difference form of the equations are presented, together with the initializations used for all the variables. The procedure for solving the resulting algebraic simultaneous equations is described and some details about the implementation of the boundary conditions are discussed. Finally, the pertinent numerical details, such as the choice of suitable time steps, the definition of convergence, etc., are presented.

Fully Implicit Scheme

After flux splitting the NS equations written in generalized coordinates, equation (25), is written as follows

$$Q'_e + E'_\xi^+ + E'_\xi^- + F'_\eta^+ + F'_\eta^- = 0 \quad (40)$$

. For details on the flux splitting used in this algorithm see reference (7:1-9). Equation (40) can be written in a factored Beam-Warming delta form as follows

$$\begin{aligned} & [I + \Delta t (\delta_\xi^- E'^+ + \delta_\xi^+ E'^-)]^n [I + \Delta t (\delta_\eta^- F'^+ + \delta_\eta^+ F'^-)]^n \Delta Q_{i,j} = \\ & - \Delta t (\delta_\xi^- E'^+ + \delta_\xi^+ E'^- + \delta_\eta^- F'^+ + \delta_\eta^+ F'^-) \Delta Q_{i,j} \end{aligned} \quad (41)$$

where

$$\delta_{\xi}^{\pm} E'_{i,j}^{\pm} = [E'_{i+1/2,j}^{\pm}(Q_{i+1/2,j}^{\pm}, M_{i+1/2,j}^{\pm}) - E'_{i-1/2,j}^{\pm}(Q_{i-1/2,j}^{\pm}, M_{i-1/2,j}^{\pm})] \quad (42)$$

$$Q_{i+1/2,j}^{-} = Q_{i,j} + \phi_{i,j}^{-} (Q_{i,j} - Q_{i-1,j}) / 2 \quad (43)$$

$$Q_{i+1/2,j}^{+} = Q_{i+1,j} - \phi_{i+1,j}^{+} (Q_{i+2,j} - Q_{i+1,j}) / 2 \quad (44)$$

The term M represents geometric terms involved in the transformation to generalized coordinates, evaluated at the cell-interface locations where the flux values are needed (7:9). The order of accuracy of the approximation is governed by the value of the switch ϕ^{-} : second order accuracy for $\phi^{-}=1$, first order for $\phi^{-}=0$ (7:4).

The terms on the left side of the equality in equation (41) are solved using first order upwind differencing, which yields a block tridiagonal system of equations. The solution of equation (41) is achieved by factorization, first solving block-tridiagonal equations in the ξ direction and then in the η direction (7:9).

The fully implicit algorithm was written assuming no slip conditions at the body surface, adiabatic wall, zero pressure gradient normal to the body (19). To start the solution using the above algorithm, some initial conditions must be assumed. Experience gained from this work shows a better initialization can be achieved, if the solution for a low Mach number, is used to initialize the flow field for a high Mach number solution. If the final solution Mach number

is very high, repeated cycles from lower to higher Mach numbers can be used. The details of this initialization will be discussed further in Chapter IV.

The Upwind Relaxation Scheme

When solving equation (30) with subsonic regions in the flow, the pressure gradient term tangent to the body allows conditions downstream to affect conditions upstream. In subsonic flow regions the pressure gradient is elliptic in nature, which would not allow the solution to be marched in the streamwise direction. To overcome this difficulty, Vigneron, Rakich and Tannehill (27) approximated the streamwise derivative term with a weighting between implicit and explicit differencing that depends on the local Mach number. The splitting of the streamwise flux term is given as follows

$$E = E^* + P \quad (45)$$

where

$$E^* = [\rho u, \rho u^2 + \omega p, \rho uv, (e_t + p)u]^T \quad (46)$$

$$P = [0, (1 - \omega)p, 0, 0]^T \quad (47)$$

$$\omega = \gamma \sigma M_\infty^2 / [1 + (\gamma - 1)M_\infty^2] \quad M_\infty < 1 \quad (48)$$

or

$$\omega = 1 \quad M_{\infty} > 1 \quad (49)$$

ω is the splitting coefficient, σ is a safety factor (17:7) and M_{∞} is the local streamwise Mach number. In order to be able to handle arbitrary geometries, the ANS equations are expressed in general coordinates ξ and η . The following coordinate transformation from physical space to computational space, are used

$$t = t \quad (50)$$

$$\xi = x \quad (51)$$

$$\eta = \eta(x, y) \quad (52)$$

such that

$$(\)_x = (\)_{\xi} \quad (53)$$

$$(\)_y = \xi_y (\)_{\xi} + \eta_y (\)_{\eta} \quad (54)$$

$$(\)_z = \eta_z (\)_{\eta} \quad (55)$$

$$\xi_z = 0 \quad (56)$$

$$J = \xi_{\alpha} \eta_{\alpha} \quad (57)$$

. This transformation simplifies the $\langle E^* \rangle$ flux vector, equation (31), in generalized coordinates to the following

$$E^{\wedge} = \langle \xi_{\alpha} E^* + \xi_{\alpha} P \rangle / J \quad (58)$$

, and equation (30) is now written as follows

$$Q'_{\alpha} + E^{\wedge}_{\xi} + F^*_{\eta} = 0 \quad (59)$$

Equation (59) is a system of nonlinear differential equations that must be linearized for the algorithm being developed to make use of well known techniques for solving systems of linear differential equations. An implicit differencing scheme will be used that repeatedly sweeps over the computational space until steady state is reached. This algorithm is similar to the work of Thomas et. al. (25), using first order backward spatial differencing on the $\langle E^* \rangle$ flux vector, first order forward spatial differencing on the $\langle P \rangle$ vector and second order implicit central spatial differencing on the $\langle E, E_{\alpha}, F_1, F_{\alpha} \rangle$ flux vectors. Using first order forward spatial differencing on the $\langle P \rangle$ vector allows conditions upstream to propagate downstream in regions of subsonic or reverse flow. The algorithm finds the difference in the $\langle Q \rangle$ vector $\langle \Delta Q \rangle$ such that

$$Q^{n+1} = Q^n + \Delta Q^n \quad (60)$$

where n represents the time level of the solution. Steady state solutions are achieved when ΔQ goes to zero.

See Appendix B for details on the linearization and differencing of equation (59), which yields the following equation

$$\begin{aligned} [A]\Delta Q_{i,j-1} + [B]\Delta Q_{i,j} + [C]\Delta Q_{i,j+1} = \\ [\xi_{\alpha} E''_{\alpha} / J] \Delta Q_{i-1,j} - \xi_{\alpha} E''_{\xi} / J - \eta_{\alpha} E_{\eta} / J + \eta_{\alpha} E''_{\eta} / J - \\ \eta_{\alpha} F_{i,\eta} / J + \eta_{\alpha} F''_{i,\eta} / J - \xi_{\alpha} P_{\xi} / J \end{aligned} \quad (61)$$

where [A],[B] and [C] are matrices defined in Appendix B, equation (b20), subscripts i and j are the grid node indices for the ξ and η directions, respectively.

Viscous Flux Vector Differencing

The viscous flux vectors (F_{η}'') contain derivatives with respect to η , and are being differenced with respect to η . Appendix B shows the differencing technique used for these terms, and the following is sample of this differencing technique. The second element in the (F_{η}'') vector is differenced as follows

$$\begin{aligned}
& [(4\mu/3\text{Re})_{i,j+1/2} + (4\mu/3\text{Re})_{i,j}] \cdot 5[\eta_x^2/J]_{i,j+1/2}^* \\
& \quad [u_{i,j+1} - u_{i,j}] / \Delta\eta^2 - \\
& [(4\mu/3\text{Re})_{i,j} + (4\mu/3\text{Re})_{i,j-1/2}] \cdot 5[\eta_x^2/J]_{i,j-1/2}^* \\
& \quad [u_{i,j} - u_{i,j-1}] / \Delta\eta^2 - \\
& [(2\mu/3\text{Re})_{i,j+1/2} + (2\mu/3\text{Re})_{i,j}] \cdot 5[\eta_x\eta_y/J]_{i,j+1/2}^* \\
& \quad [v_{i,j+1} - v_{i,j}] / \Delta\eta^2 - \\
& [(2\mu/3\text{Re})_{i,j} + (2\mu/3\text{Re})_{i,j-1/2}] \cdot 5[\eta_x\eta_y/J]_{i,j-1/2}^* \\
& \quad [v_{i,j} - v_{i,j-1}] / \Delta\eta^2 \quad (62)
\end{aligned}$$

. It should be noted the metrics $(\eta)_x$, $(\eta)_y$ and the Jacobian are evaluated at $j+1/2$ and $j-1/2$, where as the coefficient of viscosity and Reynolds number are determined by taking their average values between adjacent grid nodal points. The metrics and Jacobian are evaluated at half nodal points.

Three grid nodal points are required to implicitly difference the viscous terms using this algorithm, which results in solving a block tridiagonal matrix to get the solution. The block tridiagonal solver used in this algorithm was written by Carlson (11).

To make the convergence faster, a variable time step over the domain is implemented similar to the work of Halim and Ghia (13). Such techniques are always used to enhance the convergence if a transient solution is not of interest.

IV Results and Discussions

Application of the algorithms described in Chapter III to a series of high speed viscous flow problems are shown in this chapter. The cases studied using the fully implicit scheme are,

- The blunt body flow
 - Supersonic viscous flow past a circular wedge
- . The cases studied using the relaxation scheme are,
- Couette flow problem
 - Supersonic flow over flat plate
- . A brief description of each problem will be followed by the results and discussion of their significance.

The Blunt Body Flow

The fully implicit algorithm is used to compute the two dimensional flow fields surrounding a circular cylinder. Although the present results are two dimensional, qualitative comparisons still can be made with the Edney experiments (9), especially near the bow shock where the flow is locally two-dimensional.

The freestream conditions for the flow are

$$\begin{array}{ll} M_{\infty}=4.6 & Re_{\infty}=10000 \\ Pr=0.72 & \gamma=1.4 \\ p_{\infty}=14.93 \text{ N/m}^2 & T_{\infty}=166.7 \text{ K} \\ D=0.3048\text{m} & T_w=555.6 \text{ K} \end{array}$$

The grid shown in Figure 1 was used for this computation and has 81 grid points in the direction tangent to the body

and 71 grid points in the direction normal to the body.

The entire flow field was initialized at the freestream conditions. It was difficult to get the solution for the blunt body problem at the freestream Mach number ($M_{\infty}=4.6$). To overcome this difficulty the solution was obtained for a lower Mach number and stepped-up to its final value over 1100 iterations. The boundary conditions included no slip velocity at the body surface and no pressure gradient normal to the body. The code was modified slightly to be able to solve for constant wall temperature.

Figure 2 shows the distribution of the nondimensional wall pressure (P_w/P_{stag}) compared to the experimental data of reference (9). Figure 3 shows the distribution of the nondimensional heat flux (Q_w/Q_{stag}) along with the boundary layer solution of reference (26). Plots of Mach contours, velocity vectors, density contours and pressure contours are shown in Figures 4-7.

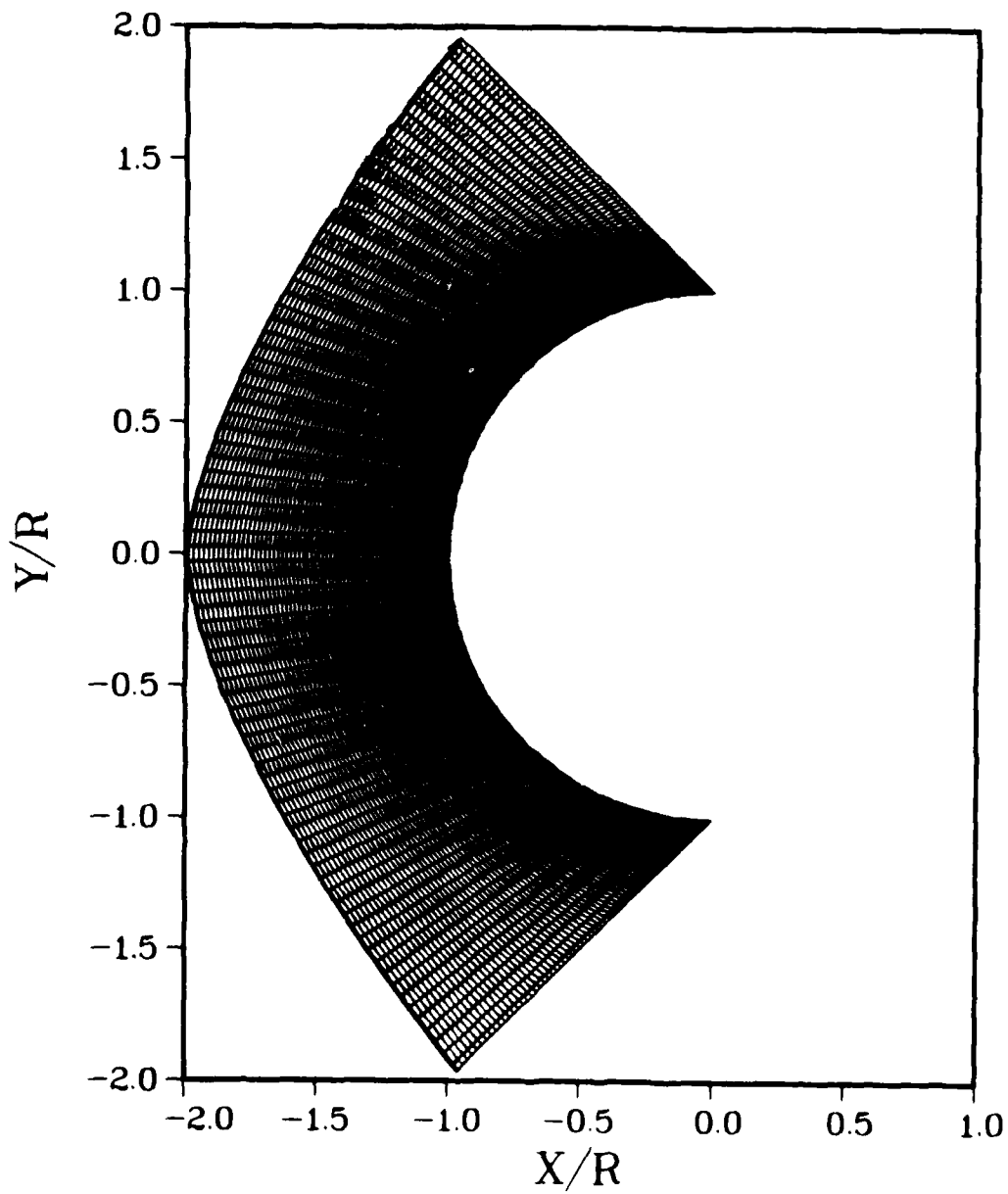


Figure 1. Typical grid for the Blunt Body problem.

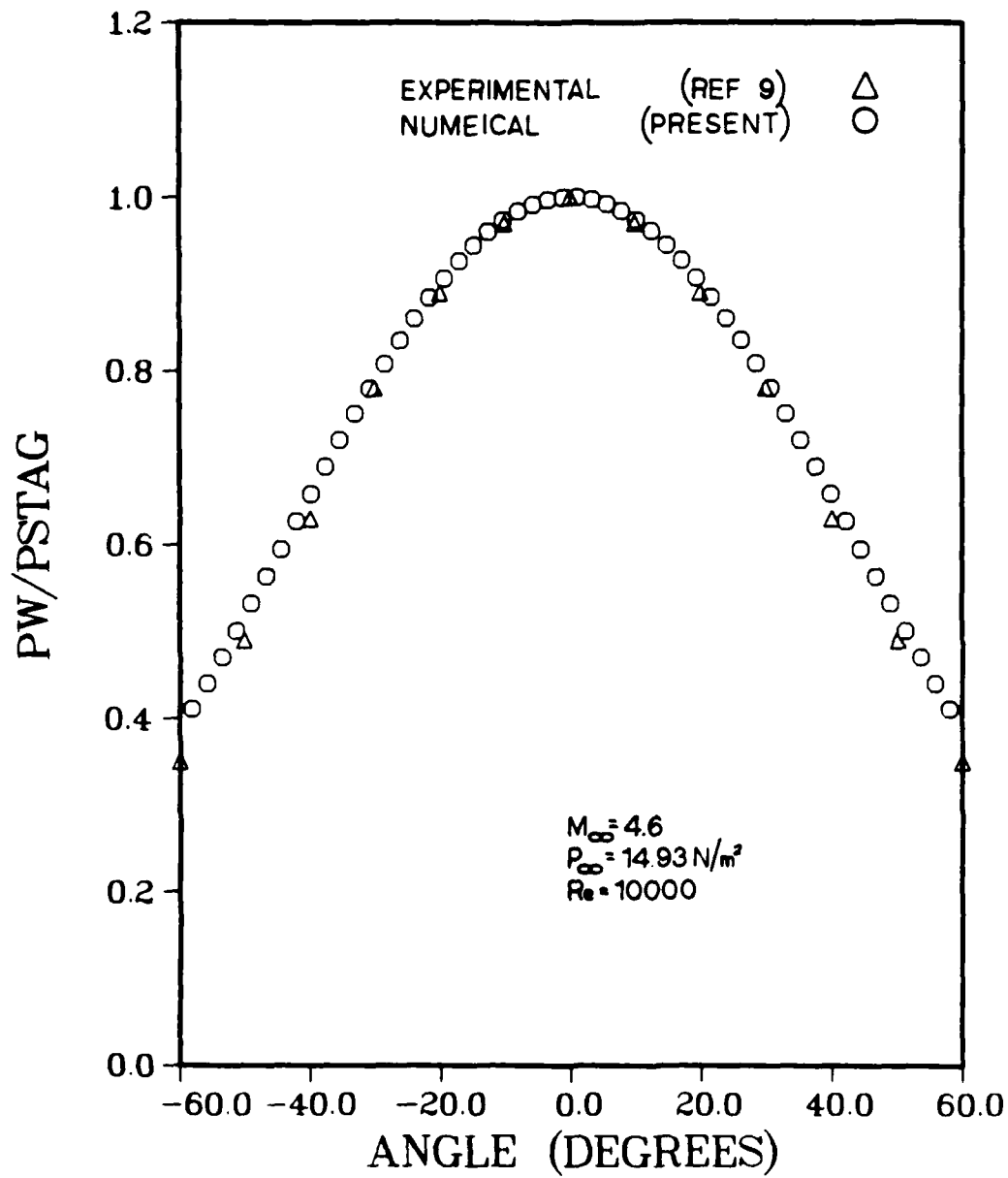


Figure 2. Comparison of Wall Pressure

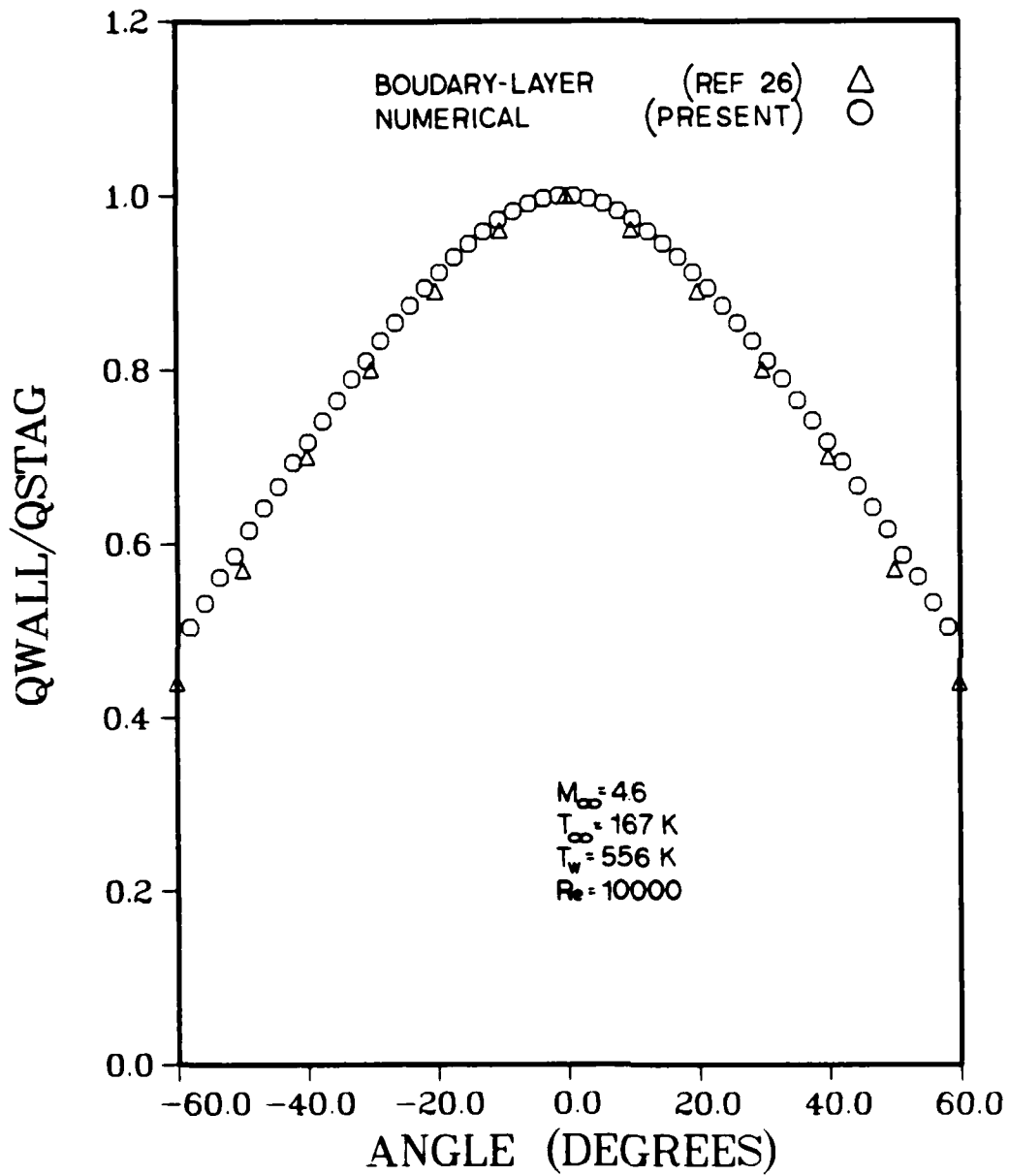


Figure 3. Comparison of Heat Flux

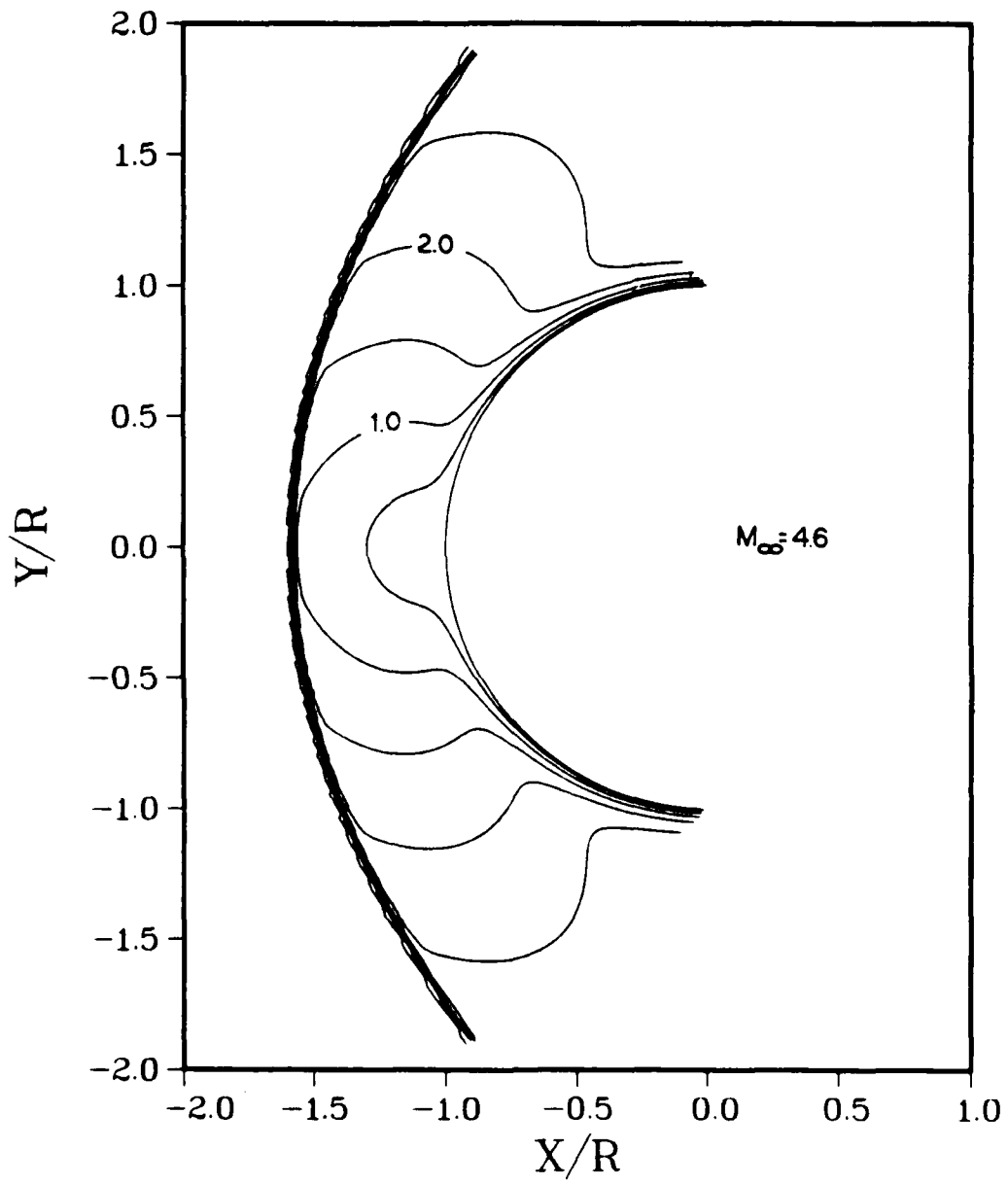


Figure 4. Mach Contours For Blunt Body

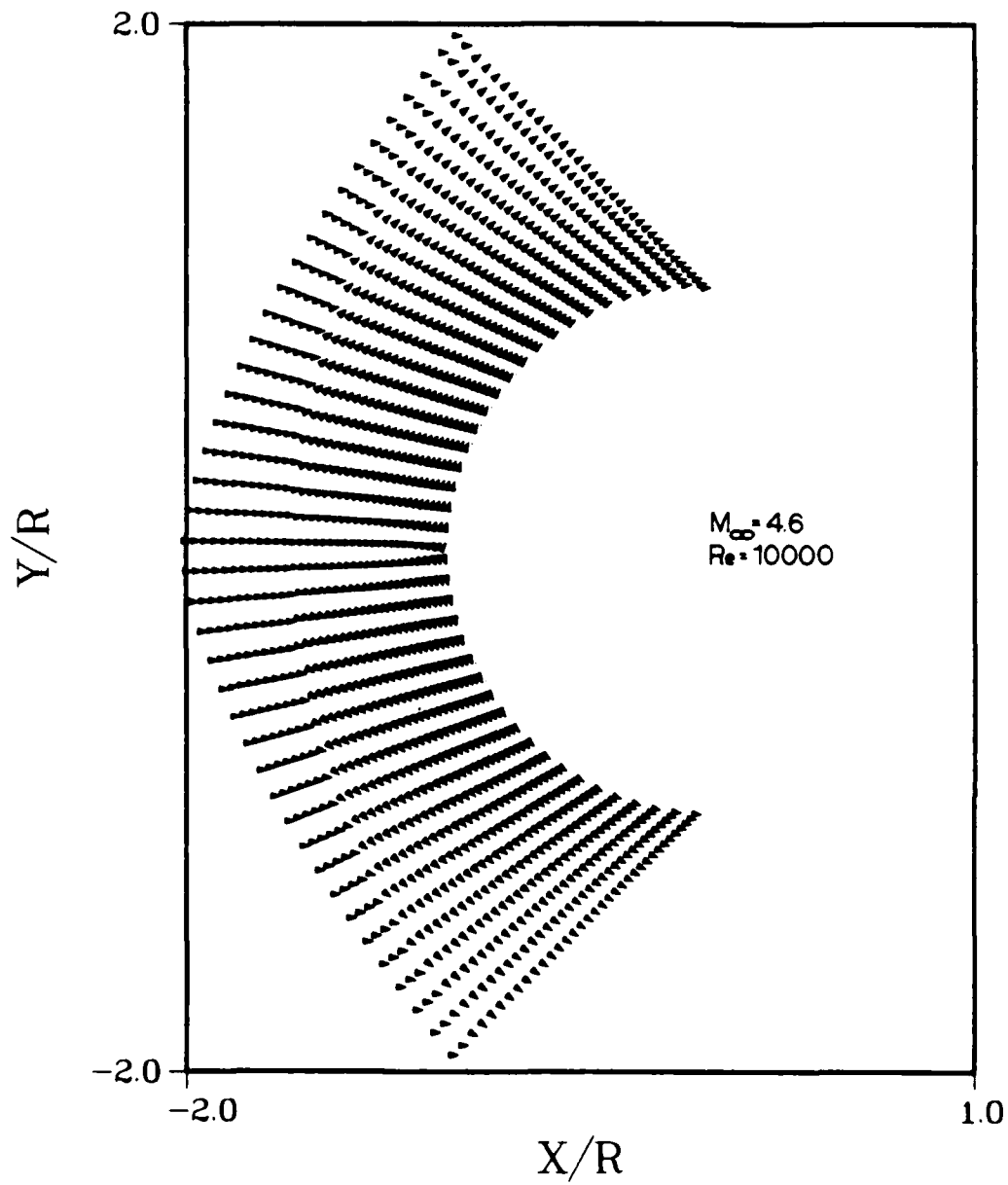


Figure 5. Velocity Vectors For Blunt Body

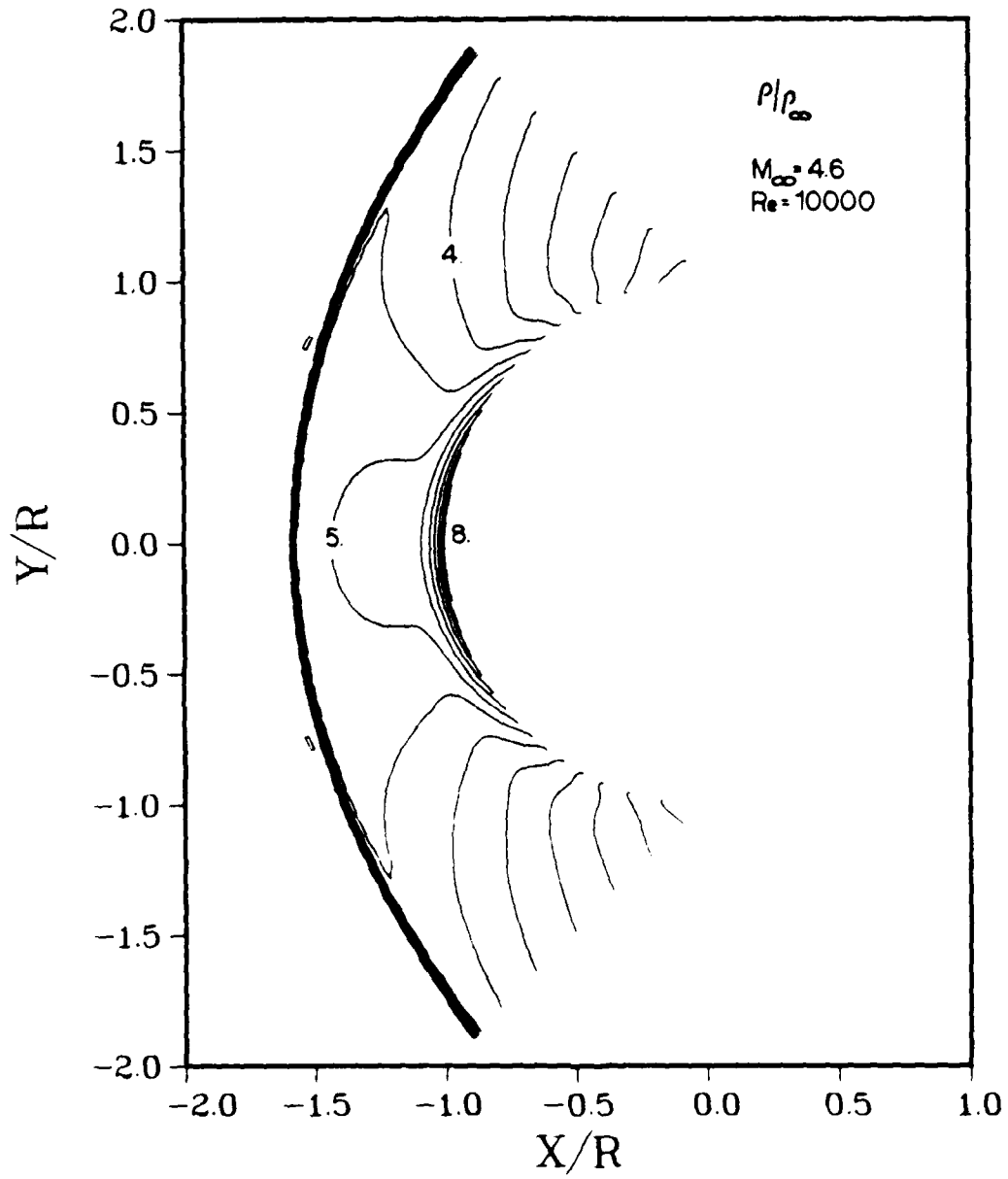


Figure 6. Density Contours For Blunt Body

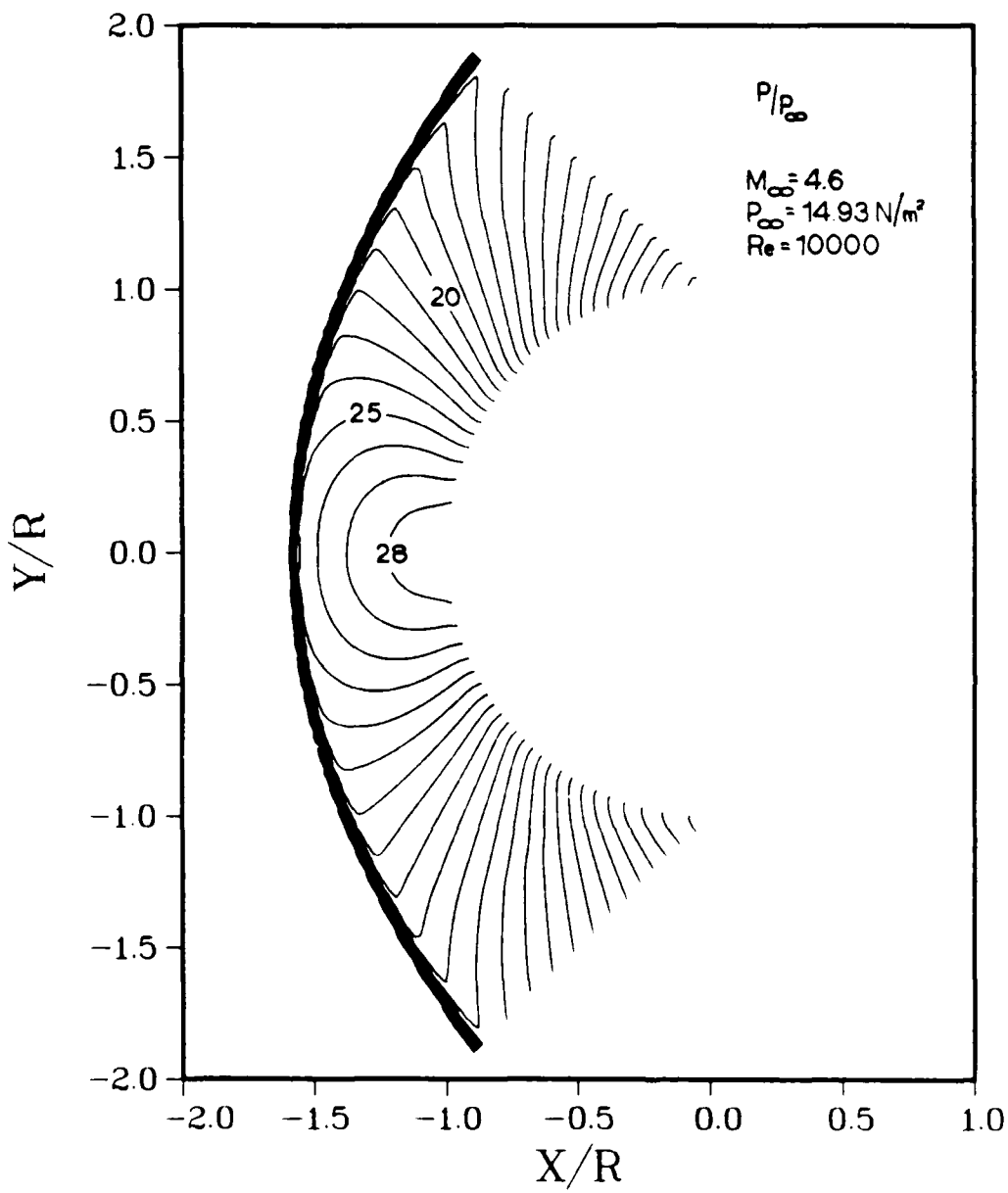


Figure 7. Pressure Contours For Blunt Body

The comparison of the wall pressure in figure 2 and the heat transfer in figure 3 show good agreement between the fully implicit algorithm and the available experimental and numerical data. That gives confidence in the algorithm to study the supersonic flow past the blunt leading edge geometry of reference (10).

Supersonic Flow Past Circular Wedge

The geometry of this problem consists of a circular cross section smoothly connected to a five degrees wedge. The Euler equations for inviscid flow over that geometry was solved by Bey et. al. (10) using the finite element approach.

The freestream conditions for the flow are

$$M_{\infty}=6.57$$

$$\gamma=1.38$$

$$D=0.75\text{in}$$

The grid used for the initial computation has 81 grid points in the direction tangent to the body and 71 grid points in the direction normal to the body. The solution for the initial computation was then used as the initial condition for the flow over a modified grid. The modified grid clustered points near the body surface to improve the resolution of the viscous layer. The modified grid shown in Figure 8 has 81 grid points tangent to the body and 62 grid points normal to the body. The grid points normal to the body have the following distribution; 32 evenly spaced grid points in the viscous layer where only 8 grid points had been

used in the unmodified grid and the remaining 30 grid points were evenly spaced normal to the body over the rest of the grid.

The entire flow field was initialized at the freestream conditions. It was difficult to get the solution for the circular wedge problem at the freestream Mach number ($M_\infty=6.57$). To overcome this difficulty the solution was obtained for a lower Mach number and stepped-up to its final value over 1100 iterations. No slip velocity are forced at the surface of the body, along with adiabatic wall and no pressure gradient normal to the body surface. Symmetry conditions were imposed along the line of symmetry.

Since the available results for this geometry are only from an inviscid solution, detailed comparison will not be possible however qualitative predictions can be seen. For example figure 9 shows the density contours using the present solution compared to those of reference (10).

Mach contours are shown in figure 10, the wall pressure is shown in figure 11, and the velocity profiles at the grid location $X/R=1$ are shown in figures 12 and 13.

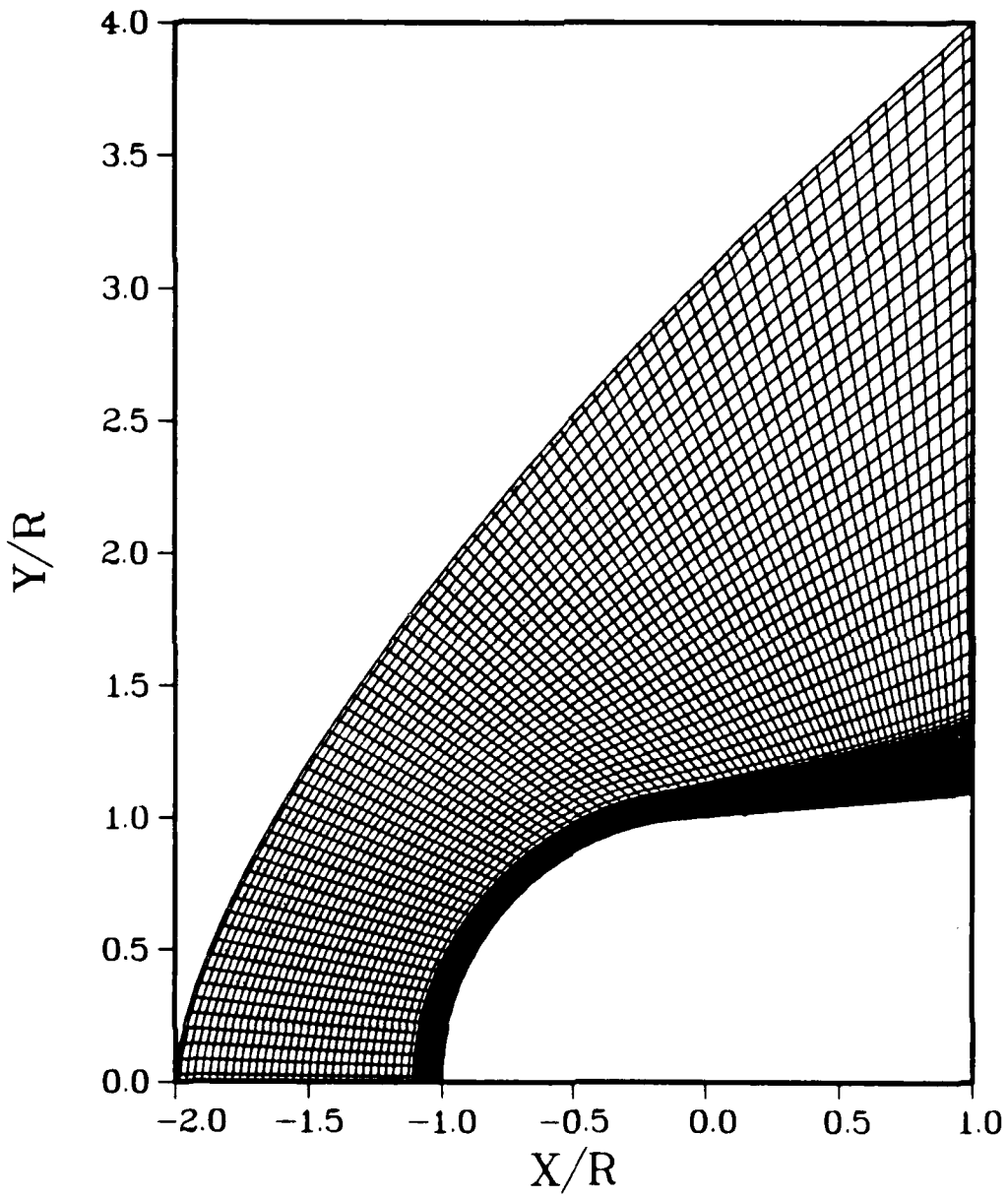


Figure 8. Clustered grid for the Circular Wedge

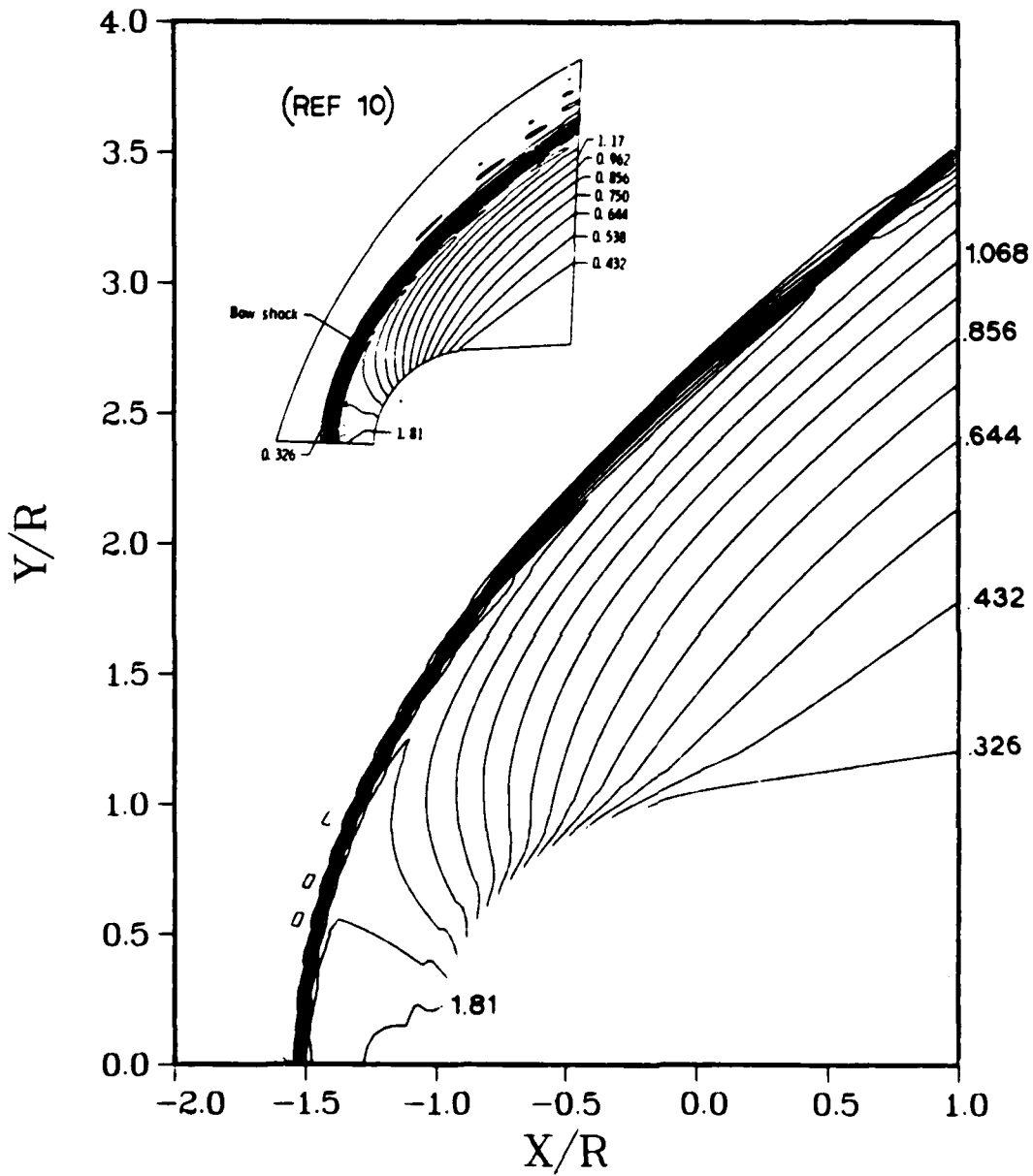


Figure 9. Density Contours For Circular Wedge
(units are $\times 10^{-6}$ lbm/in³)

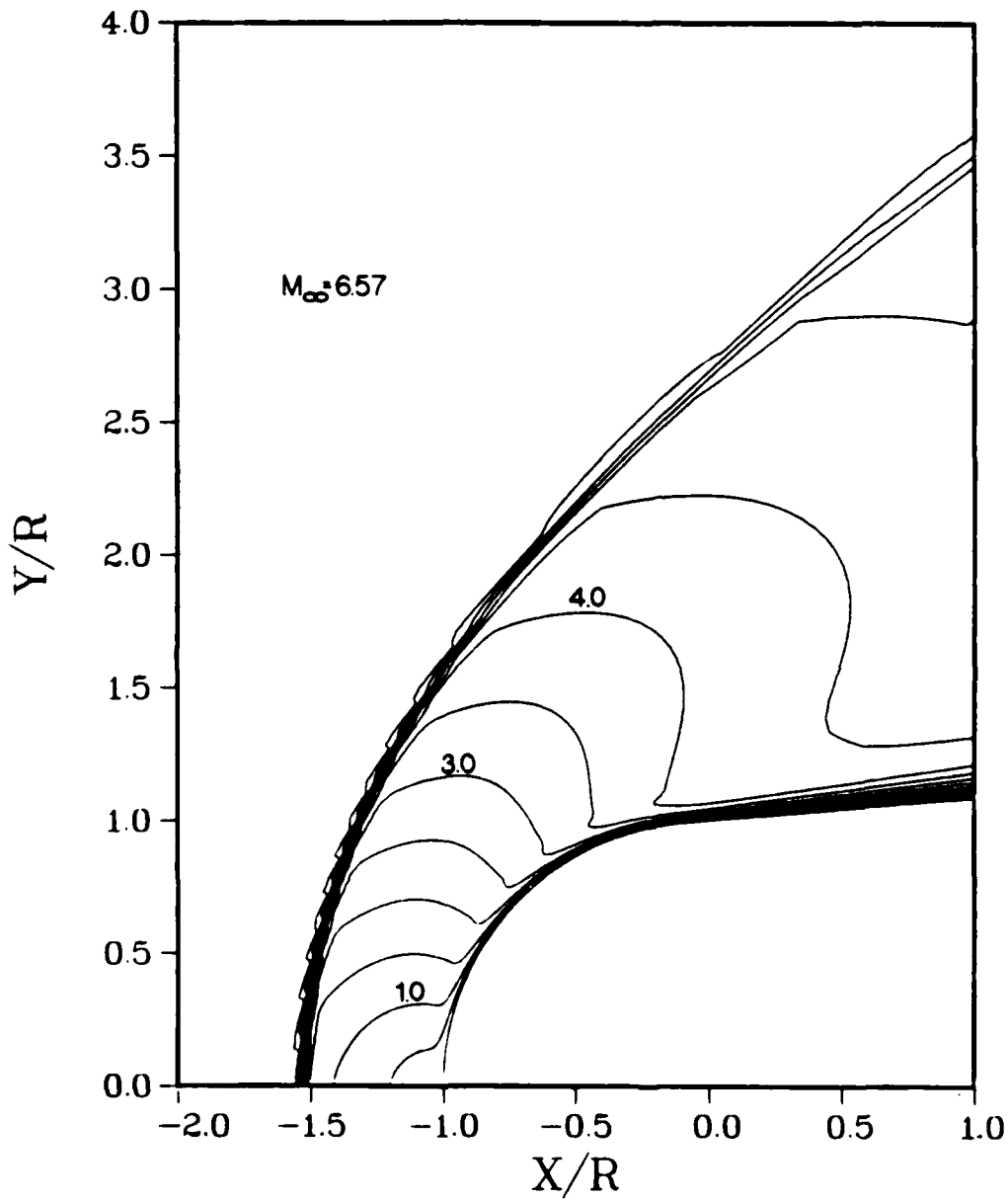


Figure 10. Mach Contours For Circular Wedge

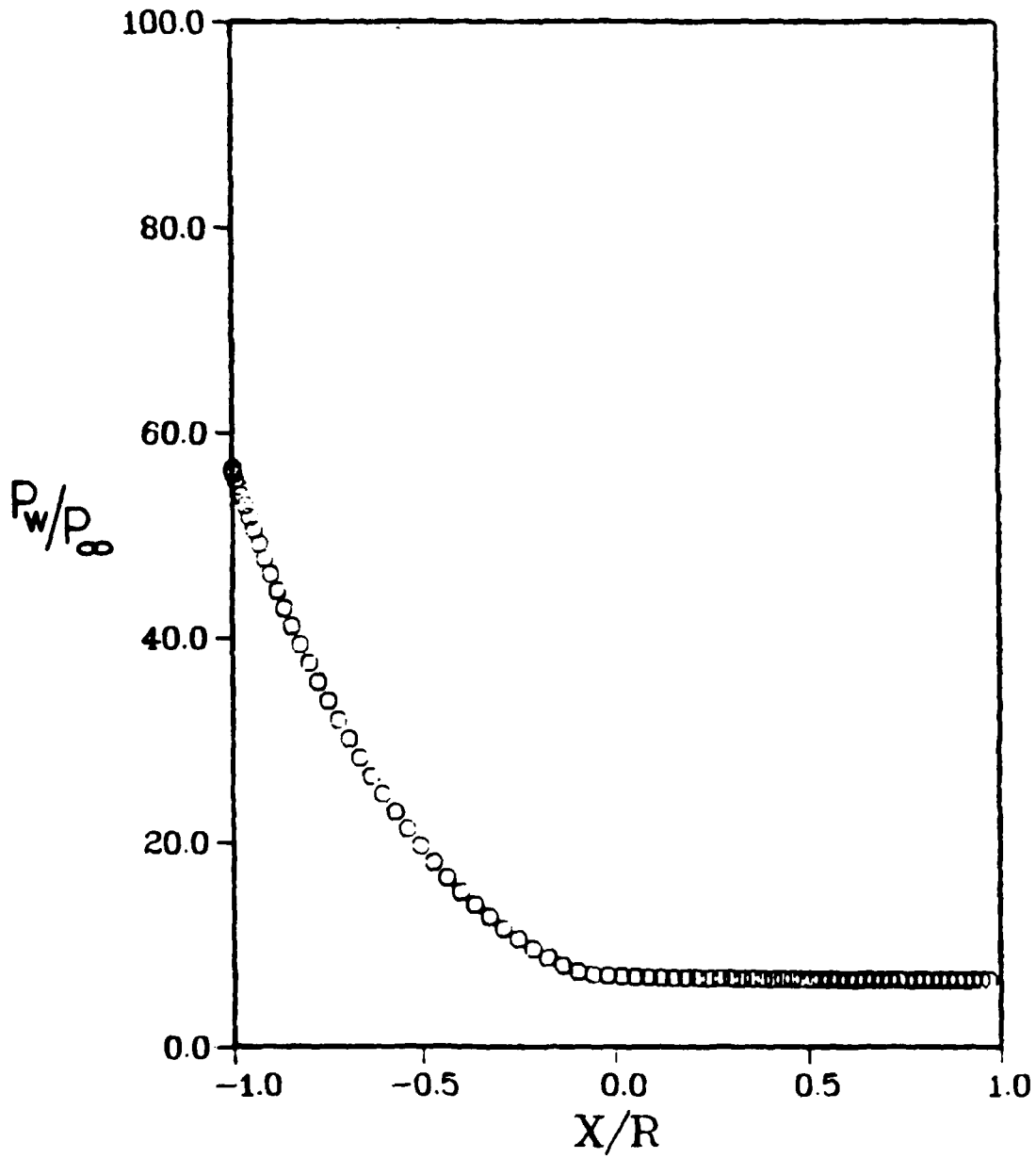


Figure 11. Wall Pressure For Circular Wedge

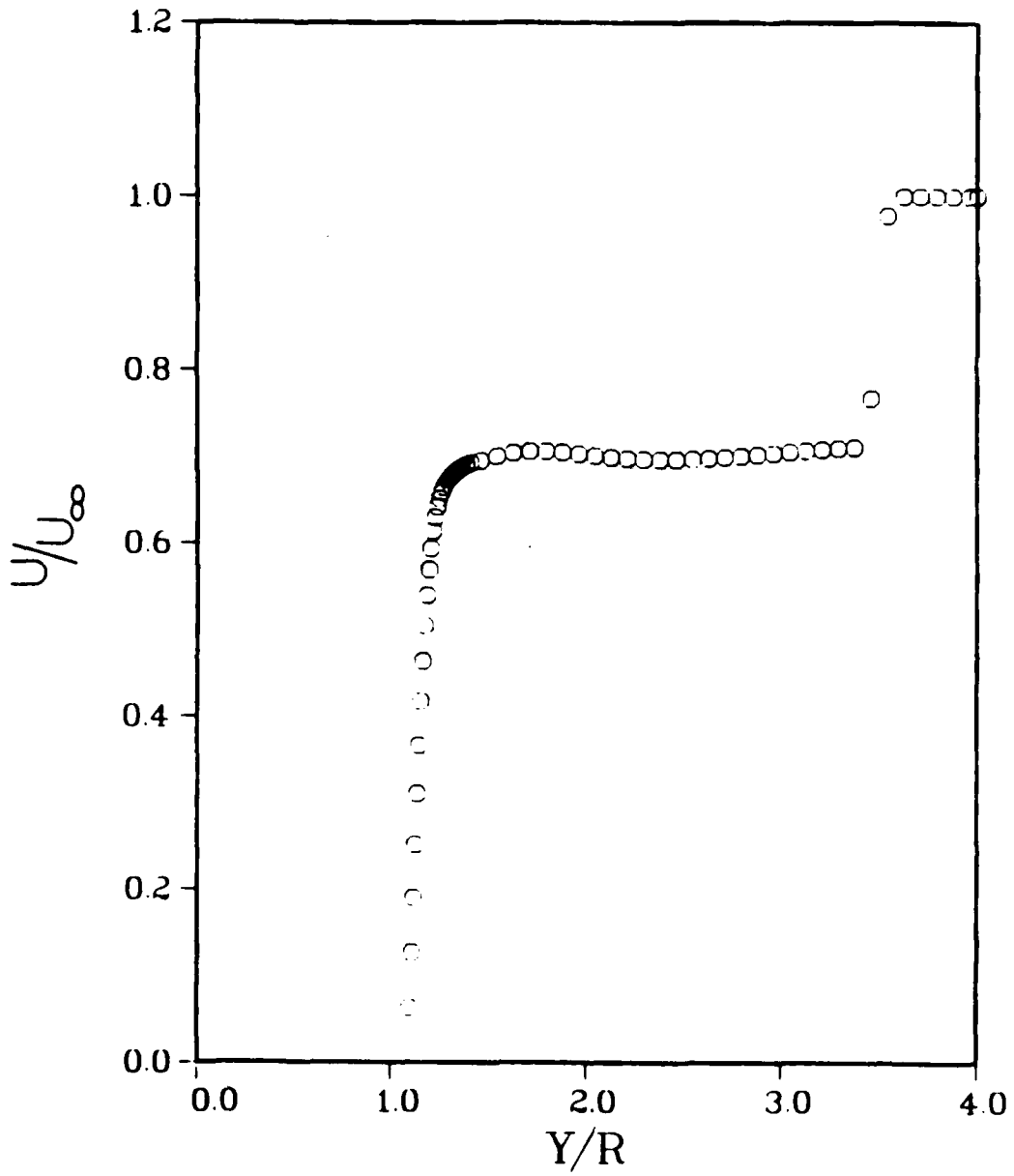


Figure 12. Distribution of the horizontal velocity at the outflow plane

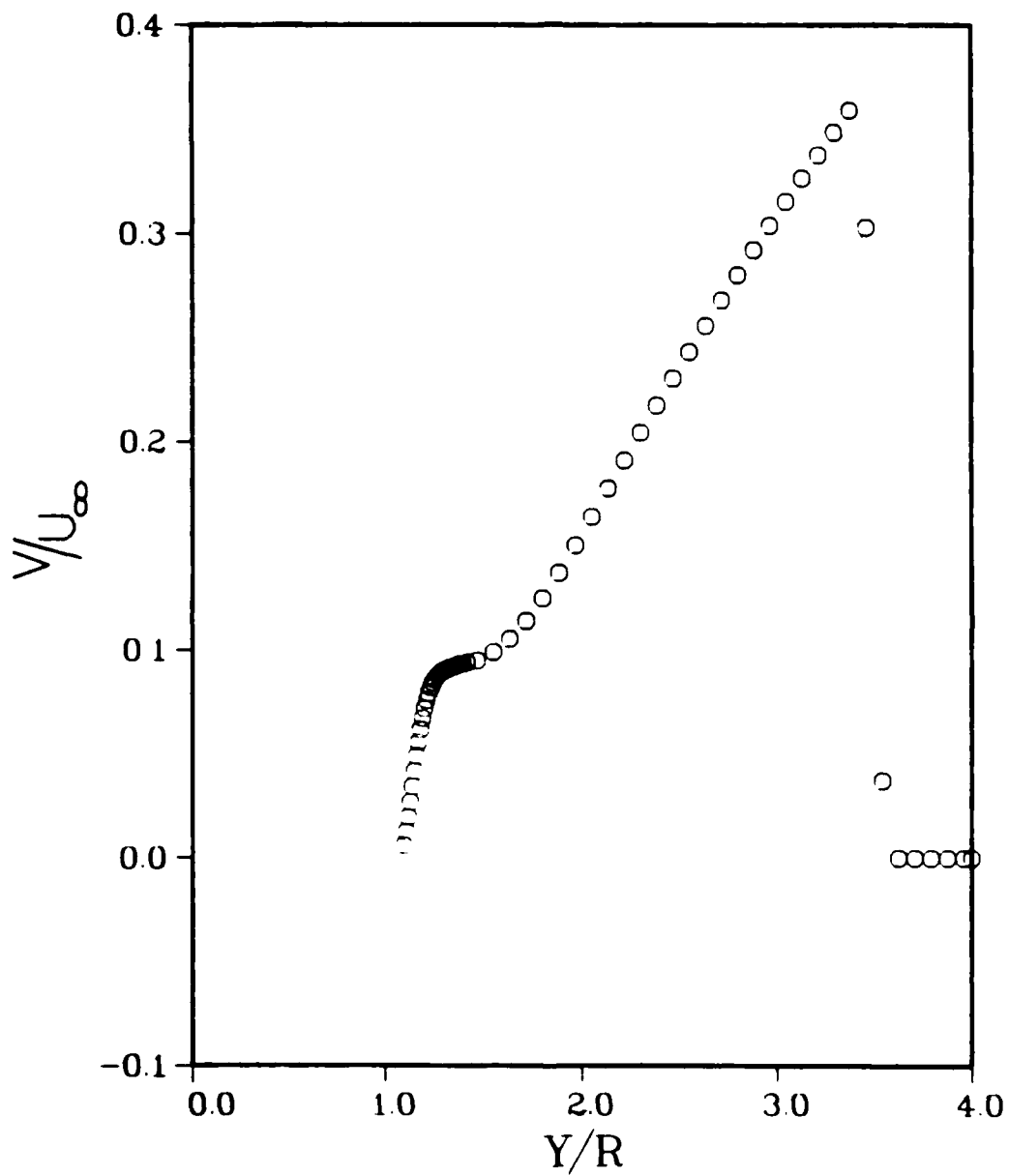


Figure 13. Distribution of the vertical velocity at the outflow plane

The next set of results are obtained using the relaxation algorithm developed in the present study.

One Dimensional Couette Flow

Couette flow is known as the flow between two infinite parallel plates separated by a distance (H). To study this flow the relaxation algorithm was solved for four pressure gradients in the direction tangent to the plates. This test case was run to check the formulation and the numerical procedures of the algorithm.

The lower plate was held fixed while the upper plate moved at Mach 0.09. The Reynolds number for this flow is 6.2, and the four pressure gradients analysed such that $B = -2, 2, 4, 7$; where $B = -(Re_H)(p)_x / [4(M_\infty^2)]$ (28:113). To convert B to correspond to nondimensionalization used in this algorithm, B' is defined where $B' = 4(M)(B)$.

The computational grid for this test case used 12 grid points in the direction normal to the plates with $y/H=1$, and the grid points in the direction tangent to the plates were varied between 10, 20 and 30 with $x/H=1$.

Initially the entire flow was given the same velocity profile and the desired pressure gradient. No slip velocity conditions are forced at the upper and lower plates, while the initial conditions at grid location $i=1$ were not allowed to change during the computation (i is the grid position index in the direction tangent to the plate).

After computing the solution for the four pressure

gradients for each of the three different x grid spacings, the solutions at grid point, $y/H=.8$ were compared (see figure 14). As the spacing between grid points decreases, the solution calculated by the algorithm should more closely approach the exact solution. Figure 14, shows that for the three x grid spacings chosen the solution agreed exactly with the analytic solution ($\Delta X = 0.0$). As a side note, although the NS equations in general do not have an exact solution, the exact solution at specific points can be obtained numerically using the accuracy study as shown in figure 14.

A comparison between the velocity profiles calculated by the algorithm and the profiles calculated using the analytical solution are presented in figure 15.

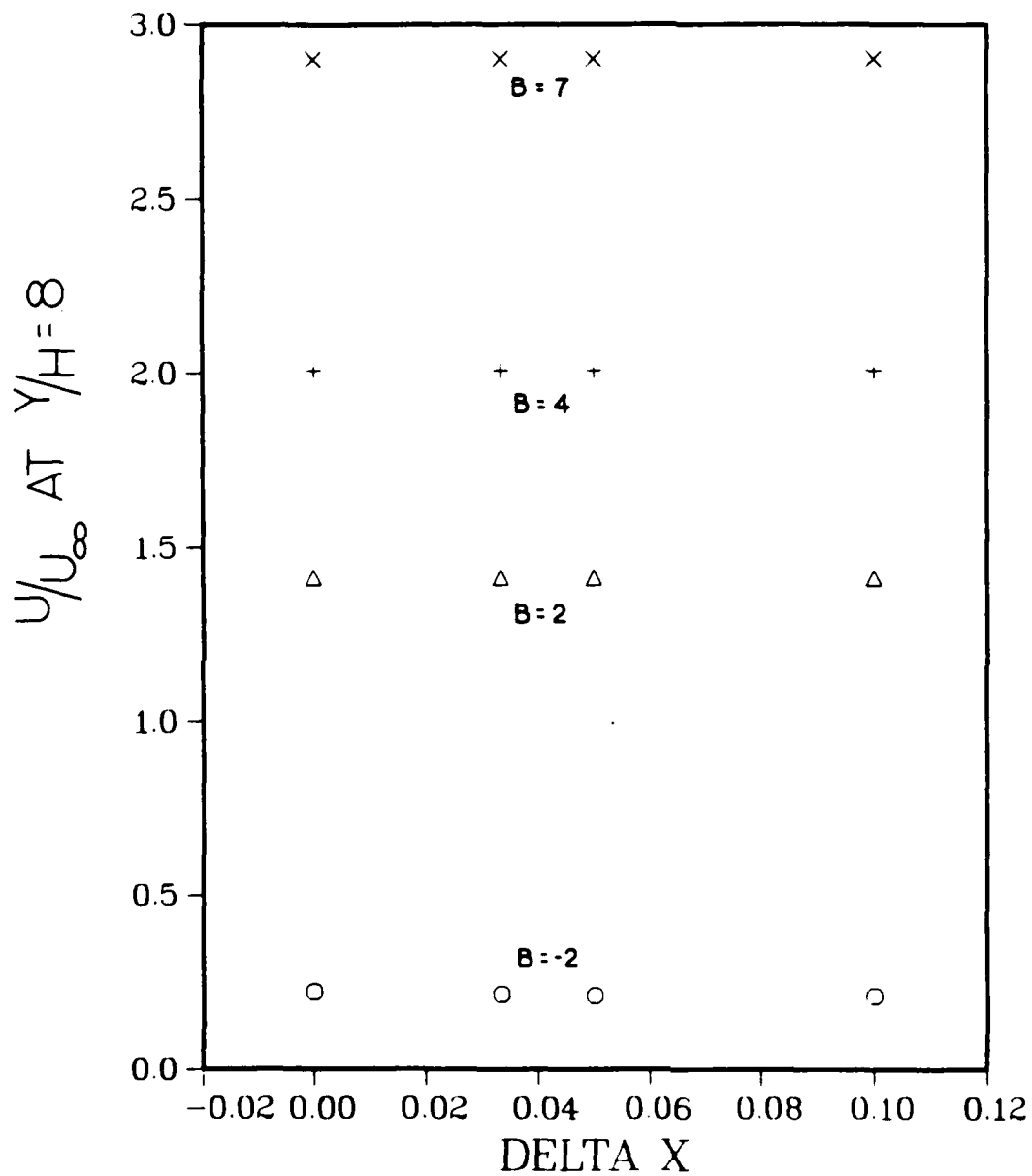


Figure 14. Accuracy study of Couette flow for different pressure gradients (B).

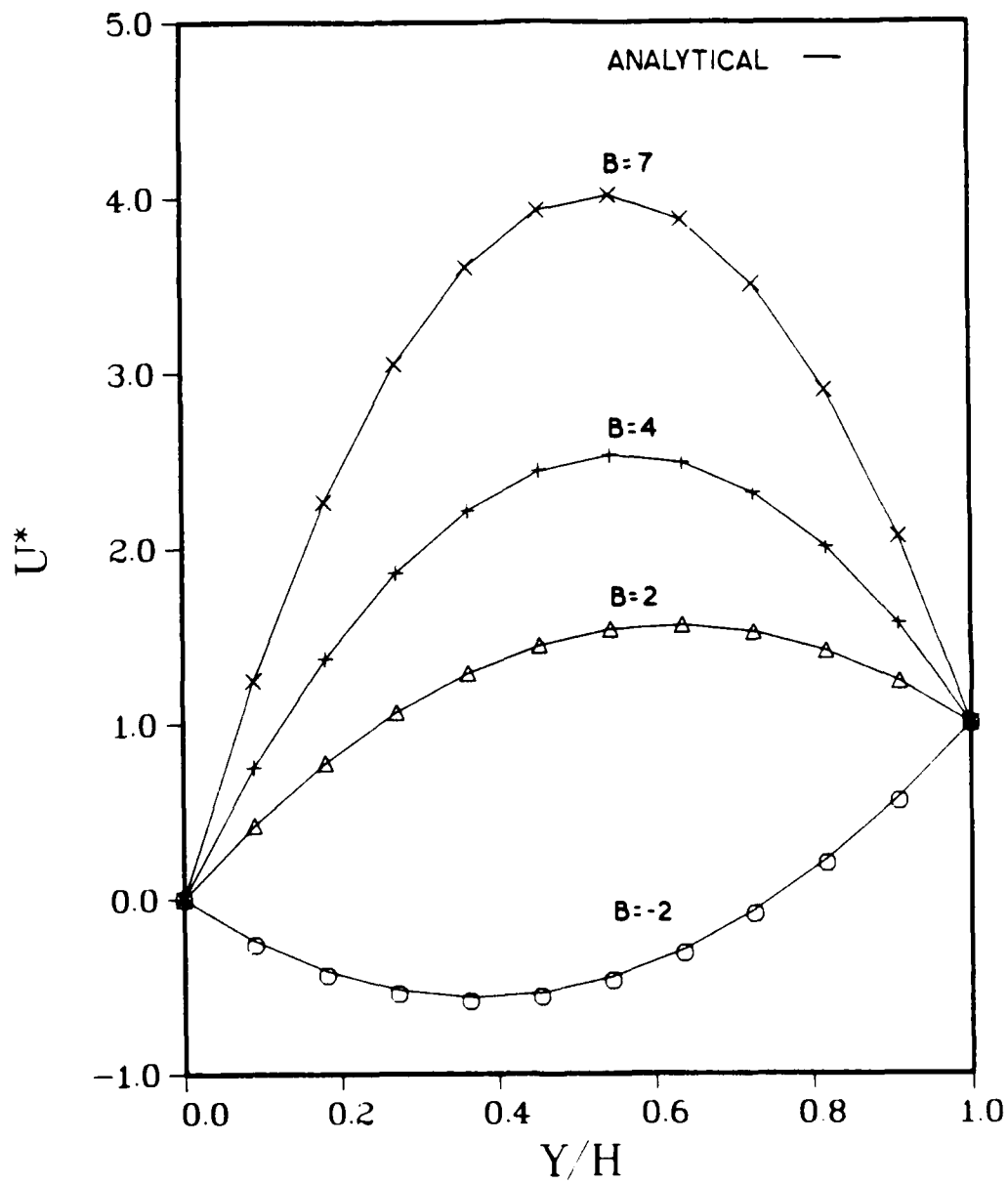


Figure 15. Velocity Profiles For Couette Flow

Supersonic Flow Over Flat Plate

The second test problem for the relaxation algorithm is solving the supersonic flow over a flat plate.

The freestream conditions for the flow are

$$M_{\infty} = 2$$

$$Re_{\infty}/L^* = 1.65 \times 10^6/m$$

$$L^* = 1m$$

$$(T_{\infty})^* = (T_w)^* = 221.6 \text{ K}$$

$$Pr = .72$$

$$\gamma = 1.4$$

The grid used 41 grid points normal to the plate surface, with a $\Delta(y) = .1524 \times 10^{-3}m$, which produced a constant grid height of $.61 \times 10^{-3}m$. The grid used 52 grid points tangent to the plate surface, with the initial grid point $i=1$ relating to the x distance of 0.305m from the leading edge of the plate. The $i=52$ grid point relating to the x distance of 0.915m from the leading edge of the plate, requiring $\Delta(x) = 0.0122m$.

The entire flow field was initialized with the velocity and temperature profiles calculated at plate position 0.305m by a boundary layer code written by Cebeci and Bradshaw (12). No slip velocity conditions were forced at the plate surface, and the normal velocity component was allowed to propagate out the top of the grid. The initial flow conditions at grid location $i=1$ were not allowed to change during the computations.

The tangential velocity and temperature profiles at

plate position 0.915m are compared to the Cebeci boundary layer solution at the same location (see figure 16 and figure 17).

As seen, relaxation algorithms would allow someone to take larger step sizes in the streamwise direction compared to space marching procedures. For example, the same problem is studied by Huband (14) using a space marching procedure. The number of points used in the streamwise direction are 612 compared to 51 used in the present study, however the CPU time taken to get the final solution using the present method is much larger compared to the space marching procedure.

U* AT X=.915 METERS

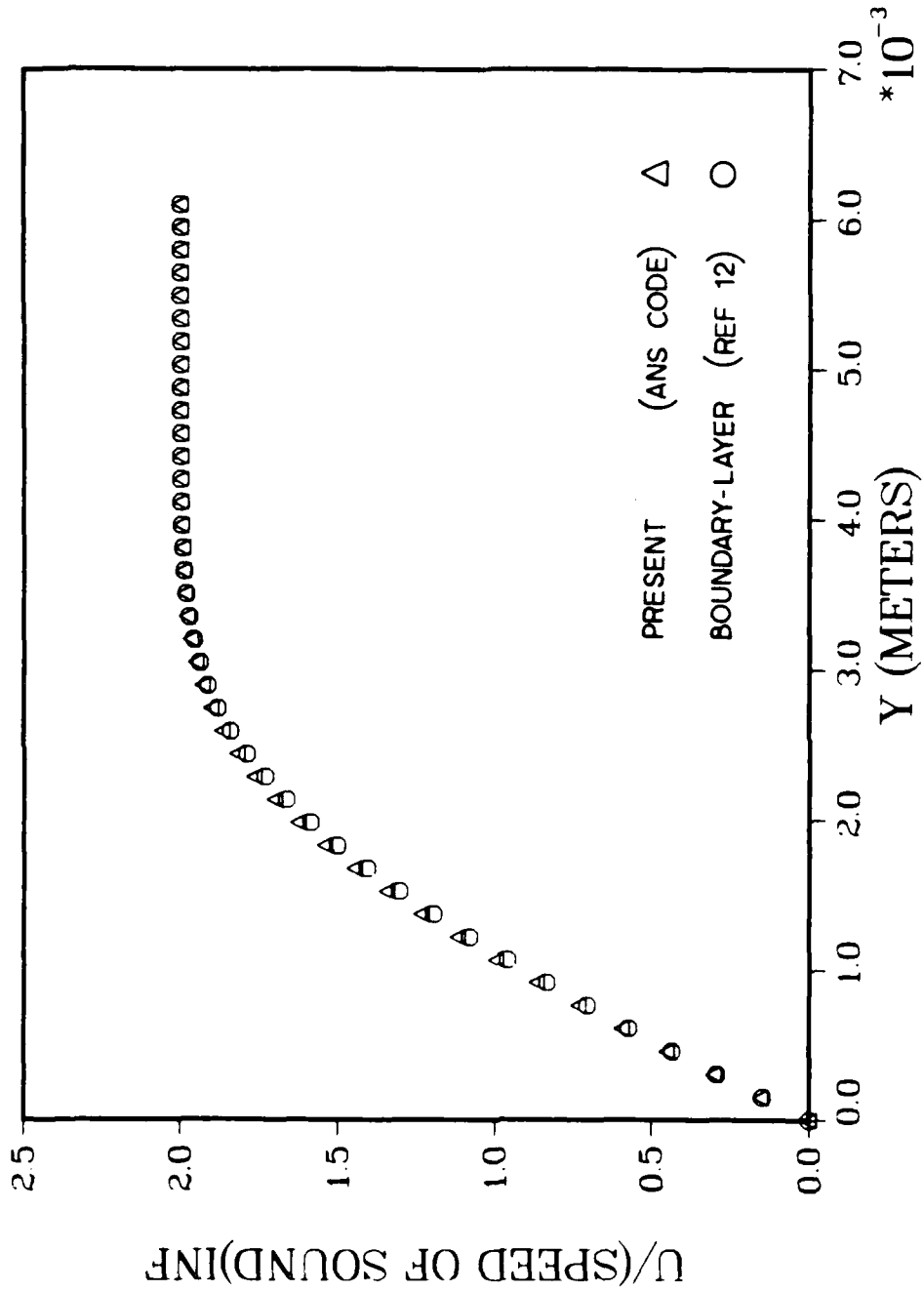


Figure 16. Comparison of Velocity Profiles For Flat Plate

T* AT X=.915 METERS

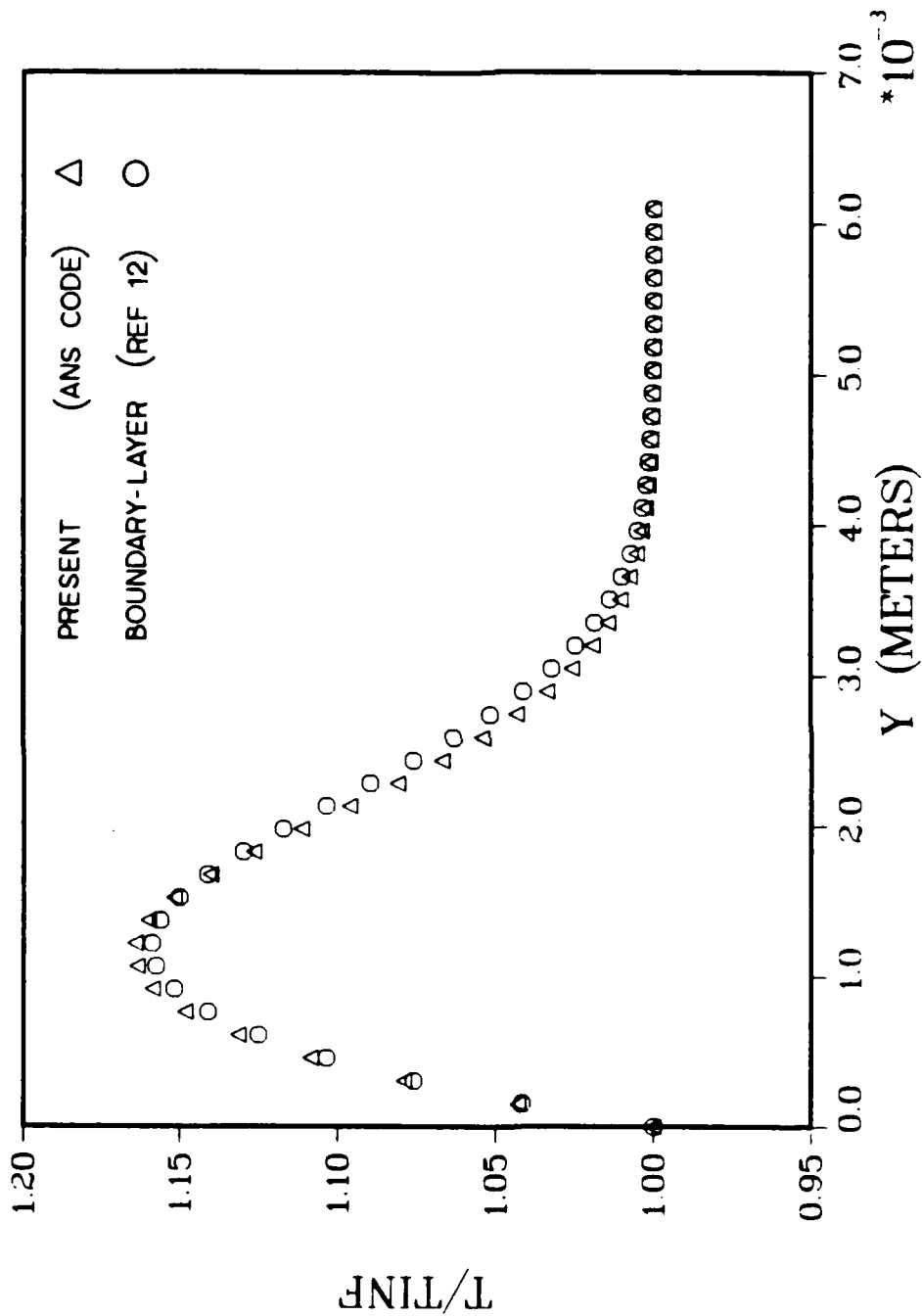


Figure 17. Comparison of Temperature Profiles For Flat Plate

V Conclusions and Recommendations

The solutions obtained using the implicit Navier-Stokes algorithm, compared favorably with experimental data. It is also recommended that this algorithm be modified to solve real gas problems.

The Approximate Navier-Stokes Algorithm developed in this study also agreed well with analytic solutions and other numeric solutions. The time required to achieve these solutions could be reduced by updating the Jacobian metrics once every five or ten iterations instead of every iteration, as was done during this study.

Appendix A: Coordinate Transformation of Governing Equations

To transform the governing equations into generalized coordinates the chain rule is used to determine the derivatives of the general coordinate variables with respect to the variables in physical space. Let the following general transforms be used

$$t = t \quad (a1)$$

$$\xi = \xi(x, y) \quad (a2)$$

$$\eta = \eta(x, y) \quad (a3)$$

with

$$(\)_t = (\)_t \quad (a4)$$

$$(\)_x = (\xi)_x (\)_\xi + (\eta)_x (\)_\eta \quad (a5)$$

$$(\)_y = (\xi)_y (\)_\xi + (\eta)_y (\)_\eta \quad (a6)$$

. The unit area in physical space is related to the unit area in the general coordinate space by the Jacobian of transformation (J). J is the determinate of the matrix formed by the metrics $(\xi)_x, (\eta)_x, (\xi)_y$ and $(\eta)_y$, which is

written as follows

$$J = (\xi_x \eta_y - \xi_y \eta_x) \quad (a7)$$

Applying the transformation to equation (16) yields

$$\begin{aligned} Q_x/J + \xi_x(E-E_v)_\xi/J + \eta_x(E-E_v)_\eta/J + \\ \xi_y(F_x-F_v)_\xi/J + \eta_y(F_x-F_v)_\eta/J = 0 \end{aligned} \quad (a8)$$

. Equation (a8) can be written in strong conservative form after applying the chain rule to each term

$$Q_x/J = (Q/J)_x - Q(1/J)_x \quad (a9)$$

$$\xi_x(E-E_v)_\xi/J = (\xi_x(E-E_v)/J)_\xi - (E-E_v)(\xi_x/J)_\xi \quad (a10)$$

$$\eta_x(E-E_v)_\eta/J = (\eta_x(E-E_v)/J)_\eta - (E-E_v)(\eta_x/J)_\eta \quad (a11)$$

$$\xi_y(F_x-F_v)_\xi/J = (\xi_y(F_x-F_v)/J)_\xi - (F_x-F_v)(\xi_y/J)_\xi \quad (a12)$$

$$\eta_y(F_x-F_v)_\eta/J = (\eta_y(F_x-F_v)/J)_\eta - (F_x-F_v)(\eta_y/J)_\eta \quad (a13)$$

and arranging terms with like derivatives as follows

$$\begin{aligned} (Q/J)_x + (\xi_x(E-E_v) + \xi_y(F_x-F_v))_\xi + (\eta_x(E-E_v) + \eta_y(F_x-F_v))_\eta \\ - Q(1/J)_x - (E-E_v)((\xi_x/J)_\xi + (\eta_x/J)_\eta) - \\ (F_x-F_v)((\xi_y/J)_\xi + (\eta_y/J)_\eta) = 0 \end{aligned} \quad (a14)$$

. The last three terms in equation (a14) are identically

zero, which can be seen after the following metrics definitions

$$\xi_x = J(\gamma) \quad (a15)$$

$$\xi_y = -J(x) \quad (a16)$$

$$\eta_x = -J(\gamma) \quad (a17)$$

$$\eta_y = J(x) \quad (a18)$$

are substituted into these last three terms. Equation (a14) can be written as follows

$$Q'_x + E'_x + F'_x = 0 \quad (a19)$$

where

$$Q' = Q/J \quad (a20)$$

$$E' = [\xi_x (E - E_\gamma) + \xi_y (F_x - F_\gamma)] / J \quad (a21)$$

$$F' = [\eta_x (E - E_\gamma) + \eta_y (F_x - F_\gamma)] / J \quad (a22)$$

The shear stress terms and the heat flux terms are transformed to general coordinates as follows

$$\tau'_{xx} = [(2\xi_x u_\xi + 2\eta_x u_\eta) - (\xi_y v_\xi + \eta_y v_\eta)] 2\mu / 3\text{Re} \quad (\text{a23})$$

$$\tau'_{xy} = [\xi_y u_\xi + \eta_y u_\eta + \xi_x v_\xi + \eta_x v_\eta] \mu / \text{Re} \quad (\text{a24})$$

$$\tau'_{yy} = [(2\xi_y v_\xi + 2\eta_y v_\eta) - (\xi_x u_\xi + \eta_x u_\eta)] 2\mu / 3\text{Re} \quad (\text{a25})$$

$$q'_x = -\mu [\xi_x T_\xi + \eta_x T_\eta] / [\text{RePr}(\gamma - 1)] \quad (\text{a26})$$

$$q'_y = -\mu [\xi_y T_\xi + \eta_y T_\eta] / [\text{RePr}(\gamma - 1)] \quad (\text{a27})$$

where

$$\text{Re} = \rho_\infty^* c_\infty^* L^* / \mu_\infty^* \quad (\text{a28})$$

$$\text{Pr} = c_p^* \mu^* / k^* \quad (\text{a29})$$

$$c_p = \gamma R / (\gamma - 1) \quad (\text{a30})$$

Appendix B: Details about the Upwind Relaxation Scheme

Linearization of the ANS Equations

To linearize equation (59) of the text

$$Q_6 + E_5^* + F_7^* = 0 \quad (b1)$$

use the following Taylor expansions

$$\begin{aligned} E^{n+1} &= E^n + \Delta \xi^n E^n \\ &= E^n + \Delta \xi^n Q_\xi E^n \\ &= E^n + \Delta Q^n E^n \end{aligned} \quad (b2)$$

where $(Q)_\xi$ can be written as $\Delta Q / \Delta \xi$, and n denotes the time level of the calculation. In like manner the linearization of the other terms are given as

$$E^{n+1} = E^n + \Delta Q^n E^n \quad (b3)$$

$$E_{\downarrow}^{n+1} = E_{\downarrow}^n + \Delta Q^n E_{\downarrow}^n \quad (b4)$$

$$F_{\downarrow}^{n+1} = F_{\downarrow}^n + \Delta Q^n F_{\downarrow}^n \quad (b5)$$

$$F_{\downarrow}^{n+1} = F_{\downarrow}^n + \Delta Q^n F_{\downarrow}^n \quad (b6)$$

. Substituting equations (b2,b3,b4,b5 and b6) into equations (58 and 32) which are then substituted into equation (b1)

yeilding

$$\begin{aligned} & \Delta Q / \Delta t / J + [\Delta Q \xi_{\alpha} E_{\alpha}^{**} / J]_{\xi} + [\Delta Q \eta_{\alpha} E_{\alpha} / J]_{\eta} - \\ & [\Delta Q \eta_{\alpha} E_{\alpha}^{**} / J]_{\eta} + [\Delta Q \eta_{\alpha} F_{\alpha} / J]_{\eta} - [\Delta Q \eta_{\alpha} F_{\alpha}^{**} / J]_{\eta} = \\ & - \xi_{\alpha} E_{\alpha}^{**} / J - \eta_{\alpha} E_{\alpha} / J + \eta_{\alpha} E_{\alpha}^{**} / J - \eta_{\alpha} F_{\alpha} / J + \eta_{\alpha} F_{\alpha}^{**} / J - \xi_{\alpha} P_{\alpha} / J \quad (b7) \end{aligned}$$

where only terms containing ΔQ are retained on the left hand side (LHS) of the equality, and these terms will be differenced implicitly at the (n+1) time level to produce a block tridiagonal matrix multiplied by the ΔQ vector at the (n) time level. The terms on the right hand side (RHS) of the equality are all known at the (n) time level.

Finite Difference Equations

The ANS equations, written in vector form in equation (b7), are differenced term by term as follows

$$\Delta Q / \Delta t / J = ([I] / \Delta t / J)_{i,j} \Delta Q_{i,j} \quad (b8)$$

$$\begin{aligned} [\Delta Q \xi_{\alpha} E_{\alpha}^{**} / J]_{\xi} = & [(\xi_{\alpha} E_{\alpha}^{**} / J)_{i,j} \Delta Q_{i,j} - \\ & (\xi_{\alpha} E_{\alpha}^{**} / J)_{i-1,j} \Delta Q_{i-1,j}] / \Delta \xi \quad (b9) \end{aligned}$$

$$\begin{aligned} [\Delta Q \eta_{\alpha} E_{\alpha} / J]_{\eta} = & [(\eta_{\alpha} E_{\alpha} / J)_{i,j+1} \Delta Q_{i,j+1} - \\ & (\eta_{\alpha} E_{\alpha} / J)_{i,j-1} \Delta Q_{i,j-1}] / 2 \Delta \eta \quad (b10) \end{aligned}$$

$$\begin{aligned}
 [\Delta Q \eta_{\times} E''_{\nu a} / J]_{\eta} &= [\beta [E''_{\nu a} \Delta Q]_{\eta}]_{\eta} = \\
 &= (\beta_{l, j} + \beta_{l, j+1}) ((E''_{\nu a})_{l, j+1} \Delta Q_{l, j+1} - (E''_{\nu a})_{l, j} \Delta Q_{l, j}) - \\
 &= (\beta_{l, j} + \beta_{l, j-1}) ((E''_{\nu a})_{l, j} \Delta Q_{l, j} - (E''_{\nu a})_{l, j-1} \Delta Q_{l, j-1}) / 2 \Delta \eta^2
 \end{aligned}
 \tag{b11}$$

$$\begin{aligned}
 [\Delta Q \eta_{\nu} F_{l a} / J]_{\eta} &= [(\eta_{\nu} F_{l a} / J)_{l, j+1} \Delta Q_{l, j+1} - \\
 &= (\eta_{\nu} F_{l a} / J)_{l, j-1} \Delta Q_{l, j-1}] / 2 \Delta \eta
 \end{aligned}
 \tag{b12}$$

$$\begin{aligned}
 [\Delta Q \eta_{\nu} F''_{\nu a} / J]_{\eta} &= [\beta [F''_{\nu a} \Delta Q]_{\eta}]_{\eta} = \\
 &= (\beta_{l, j} + \beta_{l, j+1}) ((F''_{\nu a})_{l, j+1} \Delta Q_{l, j+1} - (F''_{\nu a})_{l, j} \Delta Q_{l, j}) - \\
 &= (\beta_{l, j} + \beta_{l, j-1}) ((F''_{\nu a})_{l, j} \Delta Q_{l, j} - (F''_{\nu a})_{l, j-1} \Delta Q_{l, j-1}) / 2 \Delta \eta^2
 \end{aligned}
 \tag{b13}$$

$$\xi_{\times} E_{\xi}^* / J = (\xi_{\times} / J)_{l, j} (E_{\xi}^*_{l, j} - E_{\xi}^*_{l-1, j}) / \Delta \xi
 \tag{b14}$$

$$\eta_{\times} E_{\eta} / J = (\eta_{\times} / J)_{l, j} (E_{l, j+1} - E_{l, j-1}) / 2 \Delta \eta
 \tag{b15}$$

$$\begin{aligned}
 \eta_{\times} E''_{\nu \eta} / J &= [\beta [E''_{\nu \eta}]_{\eta}]_{\eta} = \\
 &= (\beta_{l, j} + \beta_{l, j+1}) (E''_{\nu \eta, j+1} - E''_{\nu \eta, j}) - \\
 &= (\beta_{l, j} + \beta_{l, j-1}) (E''_{\nu \eta, j} - E''_{\nu \eta, j-1}) / 2 \Delta \eta^2
 \end{aligned}
 \tag{b16}$$

$$\eta_{\nu} F_{l \eta} / J = (\eta_{\nu} / J)_{l, j} (F_{l, j+1} - F_{l, j-1}) / 2 \Delta \eta
 \tag{b17}$$

$$\begin{aligned}
 \eta_{\nu} F''_{\nu \eta} / J &= [\beta [F''_{\nu \eta}]_{\eta}]_{\eta} = \\
 &= (\beta_{l, j} + \beta_{l, j+1}) (F''_{\nu \eta, j+1} - F''_{\nu \eta, j}) - \\
 &= (\beta_{l, j} + \beta_{l, j-1}) (F''_{\nu \eta, j} - F''_{\nu \eta, j-1}) / 2 \Delta \eta^2
 \end{aligned}
 \tag{b18}$$

$$\xi \times P_{\xi} / J = (\xi \times / J)_{i,j} (P_{i+1,j} - P_{i,j}) / \Delta \xi \quad (b19)$$

where subscript (i) is the grid position index in the (ξ) direction, subscript (j) is the grid position index in the (η) direction and [I] is the identity matrix (15:447-468). Substituting equations (b8 - b13) into the terms on the left side of the equality and combining terms with identical (i,j) indices results in

$$\begin{aligned} & [-(\eta \times E_{\eta} / J)_{i,j-1} / 2\Delta \eta - (\beta_{i,j} + \beta_{i,j-1})(E''_{\eta})_{i,j-1} / 2\Delta \eta^2 - \\ & (\eta \times F_{i\eta} / J)_{i,j-1} / 2\Delta \eta - (\beta_{i,j} + \beta_{i,j-1})(F''_{\eta})_{i,j-1} / 2\Delta \eta^2] * \\ & \Delta Q_{i,j-1} + \\ & [[I] / \Delta t / J_{i,j} + (\xi \times E''_{\xi} / J)_{i,j} / \Delta \xi - (\beta_{i,j+1} + 2\beta_{i,j} + \beta_{i,j-1}) * \\ & (E''_{\xi})_{i,j} / 2\Delta \eta^2 - (\beta_{i,j+1} + 2\beta_{i,j} + \beta_{i,j-1}) / 2\Delta \eta^2] \Delta Q_{i,j} + \\ & [(\eta \times E_{\eta} / J)_{i,j+1} / 2\Delta \eta - (\beta_{i,j+1} + \beta_{i,j})(E''_{\eta})_{i,j+1} / 2\Delta \eta^2 + \\ & (\eta \times F_{i\eta} / J)_{i,j+1} / 2\Delta \eta - (\beta_{i,j+1} + \beta_{i,j})(F''_{\eta})_{i,j+1} / 2\Delta \eta^2] * \\ & \Delta Q_{i,j+1} = \text{LHS} \quad (b20) \end{aligned}$$

or

$$[A] \Delta Q_{i,j-1} + [B] \Delta Q_{i,j} + [C] \Delta Q_{i,j+1} = \text{LHS}$$

where [A],[B] and [C] are 4x4 matrices. It should be noted that term $[(\xi \times (E''_{\xi})_{\eta} / J)_{i-1,j} \Delta Q_{i-1,j}]$ was moved to the right hand side of the equality because its grid index (i-1) is at a location where ΔQ is known.

Jacobian Matrices.

Jacobian matrices, are flux vectors differentiated with respect to the (Q) vector. Before the flux vectors can be differentiated with respect to (Q), the flux vectors must be written in terms of the elements of the (Q) vector. Which is done as follows

$$Q = [\rho, \rho u, \rho v, e_t]^T = [Q_1, Q_2, Q_3, Q_4]^T \quad (b21)$$

$$E^* = [Q_2, Q_2^2/Q_1 + \omega(\gamma-1)(Q_4 - (Q_2^2 + Q_3^2)/2Q_1), Q_2 Q_3/Q_1, \\ (Q_4 + (\gamma-1)(Q_4 - (Q_2^2 + Q_3^2)/2Q_1))Q_2/Q_1]^T \quad (b22)$$

$$P = [0, (1-\omega)(\gamma-1)(Q_4 - (Q_2^2 + Q_3^2)/2Q_1), 0, 0]^T \quad (b23)$$

$$E = [Q_2, Q_2^2/Q_1 + (\gamma-1)(Q_4 - (Q_2^2 + Q_3^2)/2Q_1), Q_2 Q_3/Q_1, \\ (Q_4 + (\gamma-1)(Q_4 - (Q_2^2 + Q_3^2)/2Q_1))Q_2/Q_1]^T \quad (b24)$$

$$E^*_{\nu} = [0, \tau'_{xx}, \tau'_{xy}, u\tau'_{xx} + v\tau'_{xy} - q_x]^T \quad (b25)$$

$$\tau'_{xx} = 4\mu\eta_x(Q_2/Q_1)\eta/3Re - 2\mu\eta_y(Q_3/Q_1)\eta/3Re \quad (b26)$$

$$\tau'_{xy} = \mu\eta_y(Q_2/Q_1)\eta/Re + \mu\eta_x(Q_3/Q_1)\eta/Re \quad (b27)$$

$$q_x = \mu\gamma\eta_x[(Q_4/Q_1) - (Q_2^2 + Q_3^2)/2Q_1^2]\eta/RePr \quad (b28)$$

$$F_1 = [Q_3, Q_2 Q_3/Q_1, Q_3^2/Q_1 + (\gamma-1)(Q_4 - (Q_2^2 + Q_3^2)/2Q_1), \\ (Q_4 + (\gamma-1)(Q_4 - (Q_2^2 + Q_3^2)/2Q_1))Q_3/Q_1]^T \quad (b29)$$

$$F''_v = [0, \tau'_{xy}, \tau'_{yy}, u\tau'_{xy} + v\tau'_{yy} - q_y]^T \quad (b30)$$

$$\tau'_{yy} = 4\mu\eta_y(Q_3/Q_1)\eta/3Re - 2\mu\eta_x(Q_2/Q_1)\eta/3Re \quad (b31)$$

$$q_y = \mu\gamma\eta_y[(Q_4/Q_1) - (Q_2^2 + Q_3^2)/2Q_1]\eta/RePr \quad (b32)$$

with these definitions the Jacobian matrices can be formed as shown on the following pages.

$$(E^*)_{\mathbf{q}} = \begin{bmatrix} 11 & 12 & 13 & 14 \\ 21 & 22 & 23 & 24 \\ 31 & 32 & 33 & 34 \\ 41 & 42 & 43 & 44 \end{bmatrix} \quad (b33)$$

where

$$11 = 0$$

$$12 = 1$$

$$13 = 0$$

$$14 = 0$$

$$21 = -Q_2^2/Q_1^2 + (\omega)(\gamma-1)(Q_2^2+Q_3^2)/2Q_1^2$$

$$22 = 2Q_2/Q_1 - (\omega)(\gamma-1)Q_2/Q_1$$

$$23 = -(\omega)(\gamma-1)Q_3/Q_1$$

$$24 = (\omega)(\gamma-1)$$

$$31 = -Q_3Q_2/Q_1^2$$

$$32 = Q_3/Q_1$$

$$33 = Q_2/Q_1$$

$$34 = 0$$

$$41 = -[Q_2/Q_1^2]\{Q_4 + (\gamma-1)[Q_4 - (Q_2^2+Q_3^2)/2Q_1]\} + \\ [Q_2/Q_1][(\gamma-1)(Q_2^2+Q_3^2)/2Q_1^2]$$

$$42 = (1/Q_1)\{Q_4 + (\gamma-1)[Q_4 - (Q_2^2+Q_3^2)/2Q_1]\} - \\ (\gamma-1)(Q_2/Q_1)^2$$

$$43 = -(\gamma-1)Q_3Q_2/Q_1^2$$

$$44 = (\gamma)Q_2/Q_1$$

$$(E)_{\alpha} = \begin{bmatrix} 11 & 12 & 13 & 14 \\ 21 & 22 & 23 & 24 \\ 31 & 32 & 33 & 34 \\ 41 & 42 & 43 & 44 \end{bmatrix} \quad (b34)$$

where

$$11 = 0$$

$$12 = 1$$

$$13 = 0$$

$$14 = 0$$

$$21 = -Q_2^2/Q_1^2 + (\gamma - 1)(Q_2^2 + Q_3^2)/2Q_1^2$$

$$22 = 2Q_2/Q_1 - (\gamma - 1)Q_2/Q_1$$

$$23 = -(\gamma - 1)Q_3/Q_1$$

$$24 = (\gamma - 1)$$

$$31 = -Q_3Q_2/Q_1^2$$

$$32 = Q_3/Q_1$$

$$33 = Q_2/Q_1$$

$$34 = 0$$

$$41 = -Q_2/Q_1^2 \{ Q_4 + (\gamma - 1) [Q_4 - (Q_2^2 + Q_3^2) / 2Q_1] \} \\ + Q_2/Q_1 [(\gamma - 1)(Q_2^2 + Q_3^2) / 2Q_1^2]$$

$$42 = 1/Q_1 \{ Q_4 + (\gamma - 1) [Q_4 - (Q_2^2 + Q_3^2) / 2Q_1] \} \\ - (\gamma - 1)(Q_2/Q_1)^2$$

$$43 = -(\gamma - 1)Q_3Q_2/Q_1^2$$

$$44 = (\gamma)Q_2/Q_1$$

$$(E_{\nu''})_{\mathbf{a}} = \begin{bmatrix} 11 & 12 & 13 & 14 \\ 21 & 22 & 23 & 24 \\ 31 & 32 & 33 & 34 \\ 41 & 42 & 43 & 44 \end{bmatrix} \quad (\text{b35})$$

where

$$11 = 0$$

$$12 = 0$$

$$13 = 0$$

$$14 = 0$$

$$21 = -4(\mu)(\eta)_{\times} [Q_2/Q_1^2] \eta / 3(\text{Re}) \\ + 2(\mu)(\eta)_{\gamma} [Q_3/Q_1^2] \eta / 3(\text{Re})$$

$$22 = 4(\mu)(\eta)_{\times} [1/Q_1] \eta / 3(\text{Re})$$

$$23 = -2(\mu)(\eta)_{\gamma} [1/Q_1] \eta / 3(\text{Re})$$

$$24 = 0$$

$$31 = -(\mu)(\eta)_{\gamma} [Q_2/Q_1^2] \eta / (\text{Re}) \\ - (\mu)(\eta)_{\times} [Q_2/Q_1^2] \eta / (\text{Re})$$

$$32 = (\mu)(\eta)_{\gamma} [1/Q_1] \eta / (\text{Re})$$

$$33 = (\mu)(\eta)_{\times} [1/Q_1] \eta / (\text{Re})$$

$$34 = 0$$

$$41 = -4(\mu)(\eta)_{\times} [Q_2^2/Q_1^3] \eta / 3(\text{Re}) \\ - (\mu)(\eta)_{\times} [Q_3^2/Q_1^3] \eta / (\text{Re}) \\ + 2(\mu)(\eta)_{\gamma} [(Q_2/Q_1^2) (Q_3/Q_1) \eta \\ + (Q_2/Q_1) (Q_3/Q_1^2) \eta] / 3(\text{Re}) \\ - (\mu)(\eta)_{\gamma} [(Q_3/Q_1^2) (Q_2/Q_1) \eta \\ + (Q_3/Q_1) (Q_2/Q_1^2) \eta] / (\text{Re})$$

$$+ (\mu)(\gamma)(\eta)_{\times} [-(Q_4/Q_1^2) + (Q_2^2 + Q_3^2)/Q_1^3] \eta / (\text{Re})(\text{Pr})$$

$$\begin{aligned}
42 &= 4(\mu)(\eta)_{\times}[Q_2/Q_1]^2 \eta/3(\text{Re}) \\
&\quad -2(\mu)(\eta)_{\gamma}[Q_3/Q_1] \eta/3(\text{Re})Q_1 \\
&\quad +(\mu)(\eta)_{\gamma}Q_3[1/Q_1] \eta/(\text{Re})Q_1 \\
&\quad -(\mu)(\gamma)(\eta)_{\times}[Q_2/Q_1]^2 \eta/(\text{Re})(\text{Pr}) \\
43 &= (\mu)(\eta)_{\times}[Q_3/Q_1]^2 \eta/(\text{Re}) \\
&\quad +(\mu)(\eta)_{\gamma}[Q_2/Q_1] \eta/(\text{Re})Q_1 \\
&\quad -2(\mu)(\eta)_{\gamma}[1/Q_1] \eta/3(\text{Re}) \\
&\quad -(\mu)(\gamma)(\eta)_{\times}[Q_3/Q_1]^2 \eta/(\text{Re})(\text{Pr}) \\
44 &= (\mu)(\gamma)(\eta)_{\times}[1/Q_1] \eta/(\text{Re})(\text{Pr})
\end{aligned}$$

$$(F_i)_{\mathbf{q}} = \begin{bmatrix} 11 & 12 & 13 & 14 \\ 21 & 22 & 23 & 24 \\ 31 & 32 & 33 & 34 \\ 41 & 42 & 43 & 44 \end{bmatrix} \quad (\text{b36})$$

where

$$11 = 0$$

$$12 = 0$$

$$13 = 1$$

$$14 = 0$$

$$21 = -Q_3 Q_2 / Q_1^2$$

$$22 = Q_3 / Q_1$$

$$23 = Q_2 / Q_1$$

$$24 = 0$$

$$31 = -(Q_3 / Q_1)^2 + (\gamma - 1)(Q_2^2 + Q_3^2) / 2Q_1^2$$

$$32 = -(\gamma - 1)Q_2 / Q_1$$

$$33 = 2Q_3 / Q_1 - (\gamma - 1)Q_3 / Q_1$$

$$34 = (\gamma - 1)$$

$$41 = -Q_3 / Q_1^2 \{ Q_4 + (\gamma - 1) [Q_4 - (Q_2^2 + Q_3^2) / 2Q_1] \} \\ + Q_3 / Q_1 [(\gamma - 1)(Q_2^2 + Q_3^2) / 2Q_1^2]$$

$$42 = -(\gamma - 1)Q_2 Q_3 / Q_1^2$$

$$43 = 1 / Q_1 \{ Q_4 + (\gamma - 1) [Q_4 - (Q_2^2 + Q_3^2) / 2Q_1] \} \\ - (\gamma - 1)(Q_3 / Q_1)^2$$

$$44 = (\gamma)Q_3 / Q_1$$

$$\begin{aligned}
42 &= (\mu)(\eta)_{\gamma} [Q_2/Q_1]^2 \eta / (Re) \\
&\quad + (\mu)(\eta)_{\alpha} [Q_3/Q_1] \eta / (Re) Q_1 \\
&\quad - 2(\mu)(\eta)_{\alpha} Q_3 [1/Q_1] \eta / 3(Re) Q_1 \\
&\quad - (\mu)(\gamma)(\eta)_{\gamma} [Q_2/Q_1]^2 \eta / (Re)(Pr) \\
43 &= 4(\mu)(\eta)_{\gamma} [Q_3/Q_1]^2 \eta / 3(Re) \\
&\quad + (\mu)(\eta)_{\alpha} Q_2 [1/Q_1] \eta / (Re) Q_1 \\
&\quad - 2(\mu)(\eta)_{\alpha} [Q_2/Q_1] \eta / 3(Re) Q_1 \\
&\quad - (\mu)(\gamma)(\eta)_{\gamma} [Q_3/Q_1]^2 \eta / (Re)(Pr) \\
44 &= (\mu)(\gamma)(\eta)_{\gamma} [1/Q_1] \eta / (Re)(Pr)
\end{aligned}$$

Bibliography

1. Rakich J.V. and Kutler P.. "Comparison of Characteristics and Shocks Capturing Methods with Applications to the Space Shuttle Vehicle", AIAA Paper 72-191, (January 1972).
2. Kutler P., Lomax H. and Warming R.F.. "Computation of Space Shuttle Flow Fields Using Noncentered Finite Difference Schemes", AIAA Journal, Vol 11: pp 196-204 (February 1973).
3. Kutler P., Reinhardt W.A. and Warming R.F.. "Multishocked Three Dimensional Supersonic Flow Fields With Real Gas Effects", AIAA Journal, Vol 11: pp 657-664 (May 1973)
4. Weilmuenster K.J. and Hamilton H.H. II. "A Comparison of Computed Space Shuttle Orbiter Surface Pressure with Flight Measurements", AIAA Paper 82-0937, (June 1982).
5. Weilmuenster K.J. and Hamilton H.H. II. "Calculations of Inviscid Flow Over Shuttle-like Vehicles at High Angles of Attack and Comparisons with Experimental Data", NASA TP-2103, (May 1983).
6. Anderson W.K. and Thomas J.L.. "Multigrid Acceleration of the Flux Split Euler Equations", AIAA Paper 86-0274, (1986).
7. Anderson W.K. and Thomas J.L.. "A Comparison of Finite Volume Flux Vector Splittings for the Euler Equations", AIAA 23rd Aerospace Science Meeting, AIAA-85-0122: (January 1985).
8. Anderson D. A., Tannehill J. C. and Pletcher R. H.. Computational Fluid Mechanics and Heat Transfer. New York: Hemisphere Publishing Corporation, 1984.
9. Beckwith I.E. and Cohen N.B.. "Application of Similar Solutions to Calculation of Laminar Heat Transfer on Bodies with Yaw and Large Pressure Gradients in High Speed Flow", NASA TN D-625, (January 1961).
10. Bey K.S., Thornton E., Dechaumphai P. and Ranakrishan R.. "A New Finite Element Approach for Prediction of Aerothermal Loads", AIAA Paper 85-1533: (1985).

11. Carlson D.R., Private Communication. Air Force Institute of Technology, WPAFB OH, May 1986.
12. Cebeci T. and Bradshaw P.. Physical and Computational Aspects of Convective Heat Transfer. New York: Springer-Verlag, 1984.
13. Halim A., Ghia U. and Ghia K.N.. "Navier-Stokes Solutions, for Incompressible Separated Flow Past a Class of Two-Dimensional and Axisymmetric Semi-Infinite Bodies", Aerospace Engineering Report AFL 81-9-59, University of Cincinnati, Cincinnati, OH.
14. Huband G.. A Numerical Study of Supersonic Flows Using Different Techniques. MS thesis, AFIT/GA/AA/86D-8. Air Force Institute of Technology, WPAFB OH, December 1986.
15. Johnson L. W. and Riess R. D.. Numerical Analysis (Second Edition). Reading: Addison-Wesley Publishing Company, 1982.
16. Lawrence S.L., Tannehill J.C. and Chanssee D.S.. "An Upwind Algorithm for the Parabolized Navier-Stokes Equations", AIAA/ASME 4th Fluid Mechanics, Plasma Dynamics and Lasers Conference, AIAA-86-1117: (May 1986).
17. Lawrence S.L., Tannehill J.C. and Chanssee D.S.. Applicatoin of the Implicit MacCormick Scheme to the Parabolized Navier-Stokes Equations: Interim Report. Interchange No. NCA2-OR340-30. ISU-ERI-Ames-84432, ERI Project 1618, CFD9. November 1983.
18. Panton R.L.. Incompressible Flow. New York: John Wiley & Sons, Inc., 1984.
19. Rumsey C.L., Taylor S.L., Thomas J.L. and Anderson W.K.. "Application of an Upwind Navier-Stokes Code to Two-Dimensional Transonic Airfoil Flow", AIAA Paper 87-0413.
20. Rumsey C.L., Thomas J.L., Warren G.P. and Liu G.C.. "Upwind Navier-Stokes Solutions for Seperated Periodic Flows", AIAA 24th Aerospace Science Meeting, AIAA-86-0247: (January 1986)
21. Spiegel M. R.. Schaum's Outline of Theory and Problems of Advanced Mathematics for Engineers and Scientists. New York: McGraw-Hill Book Company, 1971.

22. Tannehill J.C. and Holst T.L.. "Numerical Computation of Two-Dimensional Viscous Blunt Body Flows with an Impinging Shock", AIAA Journal, Vol 14, No 2: pp 204-211.
23. Tanehill J.C. and Vigneron Y.C.. "Numerical Solution of Two-Dimensional Turbulent Blunt Body Flows with a Impinging Shock", AIAA 11th Fluid and Plasma Dynamics Conference, AIAA-78-1209: (July 1978).
24. Thomas J.L. and Salas M.. "Far-Field Boundary Conditions for Transonic Lifting Solutions to the Euler Equations", AIAA Paper 85-0020: (1985).
25. Thomas J.L. and Walters W.W.. "Upwind Relaxation Algorithms for the Navier-Stokes Equations", AIAA Paper 85-1501: (July 1985).
26. Tong H.. "Nonequilibrium Chemistry Boundary Layer Integral Matrix Procedure, User's Manual Parts I and II", Report UM-73-37, Aerotherm Corp., Mountain View, CA: (April 1973)
27. Vigneron Y.C., Rakich J.V. and Tannehill J.C.. "Calculation of Supersonic Viscous Flow over Delta Wings with Sharp Subsonic Leading Edge", AIAA Paper 78-1137, (1978).
28. White F.M.. Viscous Fluid Flow. New York: McGraw-Hill, Inc., 1974.

VITA

Captain Keith B. Jochum was born 8 August 1953 in Glencoe, Minnesota. He graduated from Glencoe Senior High School in 1971 and attended the University of Minnesota at Minneapolis until October 1972. At which time he enlisted in the United States Air Force and served as a Nuclear Weapons Specialist until July 1976. He returned to the University of Minnesota, receiving a Bachelors degree in Physics in June 1980, and a commission in the United States Air Force as a Distinguished Graduate from the Reserve Officers Training Corps. Called to active duty in August 1980, he entered the Aeronautical Engineering Undergraduate retraining program at the Air Force Institute of Technology, Wright-Patterson AFB, Ohio, from which he graduated in March 1982. He then served as a Spacecraft Attitude Analyst, at the 1000th Satellite Operations Group, Offutt AFB Nebraska, until entering the School of Engineering, Air Force Institute of Technology in May 1985.

Permanent address: Route 1, Box 49
Glencoe, Minnesota 55336

AD-A113 639

REPORT DOCUMENTATION PAGE

Form Approved
OMB No. 0704-0188

REPORT SECURITY CLASSIFICATION UNCLASSIFIED		1b. RESTRICTIVE MARKINGS	
SECURITY CLASSIFICATION AUTHORITY		3. DISTRIBUTION / AVAILABILITY OF REPORT Approved for public release; distribution unlimited.	
DECLASSIFICATION / DOWNGRADING SCHEDULE		5. MONITORING ORGANIZATION REPORT NUMBER(S)	
PERFORMING ORGANIZATION REPORT NUMBER(S) AFIT/GAE/AA/86D-4		7a. NAME OF MONITORING ORGANIZATION	
NAME OF PERFORMING ORGANIZATION School of Engineering	6b. OFFICE SYMBOL (if applicable) AFIT/ENY	7b. ADDRESS (City, State, and ZIP Code)	
ADDRESS (City, State, and ZIP Code) Air Force Institute of Technology Wright-Paterson AFB, OH 45433		9. PROCUREMENT INSTRUMENT IDENTIFICATION NUMBER	
NAME OF FUNDING / SPONSORING ORGANIZATION	8b. OFFICE SYMBOL (if applicable)	10. SOURCE OF FUNDING NUMBERS	
ADDRESS (City, State, and ZIP Code)		PROGRAM ELEMENT NO.	PROJECT NO.
		TASK NO.	WORK UNIT ACCESSION NO.

1. TITLE (Include Security Classification)
NUMERICAL STUDY OF HIGH SPEED VISCOUS FLOWS (UNCLASSIFIED)

2. PERSONAL AUTHOR(S)
Keith B. Jochum, B.S., Capt, USAF

3. TYPE OF REPORT MS Thesis	13b. TIME COVERED FROM _____ TO _____	14. DATE OF REPORT (Year, Month, Day) 1986 December	15. PAGE COUNT 67
--------------------------------	--	--	----------------------

4. SUPPLEMENTARY NOTATION

COSATI CODES			18. SUBJECT TERMS (Continue on reverse if necessary and identify by block number) COMPUTATIONAL FLUID DYNAMICS, FLUID DYNAMICS, NAVIER-STOKES EQUATIONS
FIELD	GROUP	SUB-GROUP	
20	04		

5. ABSTRACT (Continue on reverse if necessary and identify by block number)

see reverse side

Approved for public release: IAW AFR 190-1.

 J. E. V. [unclear]
 Director for Education and Professional Development
 Air Force Institute of Technology (AFIT)
 Wright-Paterson AFB, OH 45433

6. DISTRIBUTION / AVAILABILITY OF ABSTRACT <input checked="" type="checkbox"/> UNCLASSIFIED/UNLIMITED <input type="checkbox"/> SAME AS RPT <input type="checkbox"/> DTIC USERS		21 ABSTRACT SECURITY CLASSIFICATION UNCLASSIFIED	
7a. NAME OF RESPONSIBLE INDIVIDUAL Keith B. Jochum, Capt, USAF		22b TELEPHONE (Include Area Code) 513 255 5533	22c OFFICE SYMBOL AFIT/ENA

↓
Thermal deformations induced by aerodynamic heating on high speed vehicles are an important concern in design.

Since Aerodynamic heating may have a significant effect on the performance of the vehicle, ~~and~~ effective techniques for predicting the heat transfer and flow properties are required. The accuracy of numerical solutions depend on the grid used. Usually accurate prediction requires clustering of grid points near the surface of the body. Using an explicit algorithm to solve such problems results in the requirement for very small time steps ~~in order~~ to satisfy the stability bounds. Therefore, many iterations and large computer times are required to reach the steady state. To remove the time step restriction, fully implicit methods ~~have~~ been investigated. Results for high speed flow past a circular wedge using an implicit flux splitting scheme are shown. Also, viscous blunt body flows are computed, and qualitative comparisons with existing experimental data are given. In an effort to decrease the computational costs associated with the implicit algorithms for the Navier-Stokes equations, a relaxation algorithm is developed for the Approximate Navier-Stokes (ANS) equations. Results for Couette flow and supersonic flow over a flat plate are obtained using this relaxation algorithm and compared to analytical and other numerical solutions.

END

4-87

D T I C